Positive parity states in ^{208}Pb excited by the proton decay of the isobaric analog intruder resonance $j_{15/2}$ in ^{209}Bi

A. Heusler,[1,*] G. Graw,[2] R. Hertenberger,[2] F. Riess,[2] H.-F. Wirth,[2] T. Faestermann,[3] R. Krücken,[3] T. Behrens,[3] V. Bildstein,[3] K. Eppinger,[3] C. Herlitzius,[3] O. Lepyoshkina,[3] M. Mahgoub,[3] A. Parikh,[3] S. Schwertel,[3] K. Wimmer,[3] N. Pietralla,[4] V. Werner,[5] J. Jolie,[6] D. Mücher,[6] C. Scholl,[6] and P. von Brentano[6]

[1]*Max-Planck-Institut für Kernphysik, D-69029 Heidelberg, Germany*
[2]*Fakultät für Physik, Ludwig-Maximilians–Universität München, D-85748 Garching, Germany*
[3]*Physik Department E12, Technische Universität München, D-85748 Garching, Germany*
[4]*Institut für Kernphysik, Technische Universität Darmstadt, D-64289 Darmstadt, Germany*
[5]*Wright Nuclear Structure Laboratory, Yale University, New Haven, Connecticut 06520-8120, USA*
[6]*Institut für Kernphysik, Universität zu Köln, D-50937 Köln, Germany*

(Received 14 February 2010; revised manuscript received 11 May 2010; published 26 July 2010)

With the Q3D magnetic spectrograph of the Maier-Leibnitz-Laboratorium at München at a resolution of about 3 keV, angular distributions and excitation functions of the reaction ^{208}Pb(p,p') were measured at some scattering angles 20°–138° for several proton energies 14.8–18.1 MeV. All seven known isobaric analog resonances in ^{209}Bi are covered. By the excitation near the $j_{15/2}$ intruder resonance in ^{209}Bi, several new positive parity states in ^{208}Pb with excitation energies 4.6–6.2 MeV are identified by comparison of the mean cross section to the known single particle widths. The dominant configuration for 27 positive parity states is determined and compared to the schematic shell model.

DOI: 10.1103/PhysRevC.82.014316 PACS number(s): 21.10.Hw, 21.60.Cs, 24.30.Gd, 27.80.+w

I. INTRODUCTION

The method of inelastic proton scattering via isobaric analog resonances in ^{209}Bi (IAR-pp') allows to determine the complete neutron particle-hole structure of nuclear states in ^{208}Pb [1–4]. In the reaction ^{208}Pb(p,p') the particle of a particle-hole configuration is chosen by adjusting the proton energy E_p to the appropriate isobaric analog resonance (IAR) in ^{209}Bi. The excitation energy of the particle-hole state is obtained from the energy $E_{p'}$ of the inelastically scattered proton. The configuration amplitudes of the holes, coupling to the particle, are determined from the angular distribution of the outgoing protons in the reaction ^{208}Pb(p,p') (see [5] and references therein).

In the doubly magic nucleus ^{208}Pb, the shell model predicts the majority of particle-hole states to have negative parity. However above and below each major gap among the shell model orbits ($N = 126$, $Z = 82$), there is an intruder with a parity different from the regular orbits. Therefore in ^{208}Pb some positive parity states have similar low excitation energies as negative parity states.

Indeed in ^{208}Pb below $E_x = 6.1$ MeV, the schematic shell model without residual interaction (SSM) predicts 36 one-particle one-hole (1p-1h) states with spins 5^+–10^+. In the *Nuclear Data Sheets* [6] (in the following often called NDS2007) only about 30 states with positive parity are known and much less states with spins 5^+–10^+. We add nearly a dozen more states to the number of firmly identified positive parity states.

In principle, the parity of a particle-hole state in ^{208}Pb can be determined in a straightforward manner by measuring excitation functions of the inelastic proton scattering on ^{208}Pb via IAR in ^{209}Bi. Namely only the proton decay of the *intruder* IAR $j_{15/2}$ is calculated to populate positive parity particle-hole state with measurable cross sections; in all other IAR very low cross sections for particle-hole configurations with the *intruder hole* $i_{13/2}$ are predicted [7]. Indeed, early measurements of excitation functions identified the lowest 8^+ in ^{208}Pb to be selectively excited by the $j_{15/2}$ IAR [4].

By IAR-pp', states with dominant *proton* particle-hole configurations are observed via an *admixture of neutron* particle-hole configurations. Therefore almost all states in ^{208}Pb may be detected by ^{208}Pb(p,p') via IAR in ^{209}Bi.

The method of inelastic proton scattering via IAR developed after 1965 [1–4,8] gave the impetus to construct the Q3D magnetic spectrograph in the 1970s at several labs. At the Maier-Leibnitz-Laboratorium of the LMU München and the TU München, the Q3D magnetic spectrograph was improved during a long period [9,10]. But finally only the detector constructed in 1999 allowed for the resolution needed to resolve most states in ^{208}Pb [11]. Namely the mean distance between two levels in ^{208}Pb for $E_x = 4.5$–6.2 MeV is about 10 keV and before 1999 the best resolution was only 4 keV [12].

So the method of inelastic proton scattering via IAR was resumed in 2003 [5] after the high resolution particle spectroscopy has matured. With a resolution of about 3 keV, the Q3D magnetic spectrograph at München allows to measure excitation functions and angular distributions of IAR-pp' for states in ^{208}Pb with excitation energies $2.5 < E_x < 8.2$ MeV. In favorable regions and at scattering angles $20° \leqslant \Theta \leqslant 138°$, cross section as low as $0.5\,\mu$b/sr with a background of $0.1\,\mu$b/sr can be measured in typically half an hour with sufficient statistics.

Results for states populated strongly by the $i_{11/2}$ IAR in ^{209}Bi are shown in [5]. Here we present results for more

*A.Heusler@mpi-hd.mpg.de

than 30 states in ^{208}Pb below $E_x = 6.1$ MeV with mean cross sections of 0.5–25 μb/sr excited in the $j_{15/2}$ IAR. Some doublets with less than 5 keV distance are resolved and several new states are identified. Positive and negative parity is determined unambiguously. Preliminary results were already presented at conferences [13,14] and included in [5,6].

Angular distributions are measured but the full analysis is not presented here, essentially only the mean cross sections are used. The complete transformation matrix from the SSM configuration space to the real states in ^{208}Pb can be determined by using the data from angular distributions and the assumption of an unitary transformation matrix. The method has been successfully applied to determine the structure of generalized neutron particle-hole states in ^{140}Ce [8] and of the lowest negative parity states in ^{208}Pb [16,17]. For the positive parity states with spins 5^+–10^+ in ^{208}Pb, however, a detailed discussion would become lengthy.

In Secs. II A and II B shell model states are discussed, in Sec. II C shortly the method of IAR-pp'. The experimental determination of excitation energies from the Q3D experiments is discussed in Sec. III B. In Sec. III C excitation functions of ^{208}Pb(p, p') are discussed yielding new resonance parameters for the $j_{15/2}$ IAR (Sec. III F). The disentangling of several doublets with spacings of less than 5 keV among more than 120 states observed below $E_x = 6.1$ MeV is discussed in Sec. III D. Results are given in Sec. IV.

II. THEORY

A. Basic configurations

1. Schematic shell model

In the SSM the energies E_x of states in ^{208}Pb ($A = 208$) with one-particle one-hole (1p-1h) structure are derived from the masses m of the four neighboring nuclei [18] and the excitation energies $E_x^{\rm expt}$ of the particle LJ in ^{209}Bi and of the hole lj in ^{207}Tl for protons (π), of the particle LJ in ^{209}Pb and of the hole lj in ^{207}Pb for neutrons (ν) determined from experiment [15],

$$\begin{aligned} E_x^{\rm SSM}(\pi, LJ, lj) &= \Delta E_C(A, Z) + \Delta Q(A, Z, \pi)c^2 \\ &\quad + E_x^{\rm expt}(\pi, LJ) + E_x^{\rm expt}(\pi, lj), \\ E_x^{\rm SSM}(\nu, LJ, lj) &= \Delta E_C(A, N) + \Delta Q(A, N, \nu)c^2 \\ &\quad + E_x^{\rm expt}(\nu, LJ) + E_x^{\rm expt}(\nu, lj), \end{aligned} \tag{1}$$

where

$$\begin{aligned} \Delta Q(A, Z, \pi) &= m(^{208}\text{Bi}, LJ_{\rm g.s.}) - m(^{208}\text{Pb}, 0^+_{\rm g.s.}) \\ &\quad + m(^{207}\text{Tl}, lj_{\rm g.s.}) - m(^{208}\text{Pb}, 0^+_{\rm g.s.}) \\ &= 4214 \text{ keV} \text{ is the magic gap at } Z = 82, \\ \Delta Q(A, N, \nu) &= m(^{209}\text{Pb}, LJ_{\rm g.s.}) - m(^{208}\text{Pb}, 0^+_{\rm g.s.}) \\ &\quad + m(^{207}\text{Pb}, lj_{\rm g.s.}) - m(^{208}\text{Pb}, 0^+_{\rm g.s.}) \\ &= 3431 \text{ keV is the magic gap at } N = 126. \end{aligned} \tag{2}$$

Figure 1 shows the excitation energies in ^{209}Pb, ^{207}Pb, ^{209}Bi, ^{207}Tl and the magic gaps ΔQ. In this paper positive parity states built with particle-hole configurations are discussed

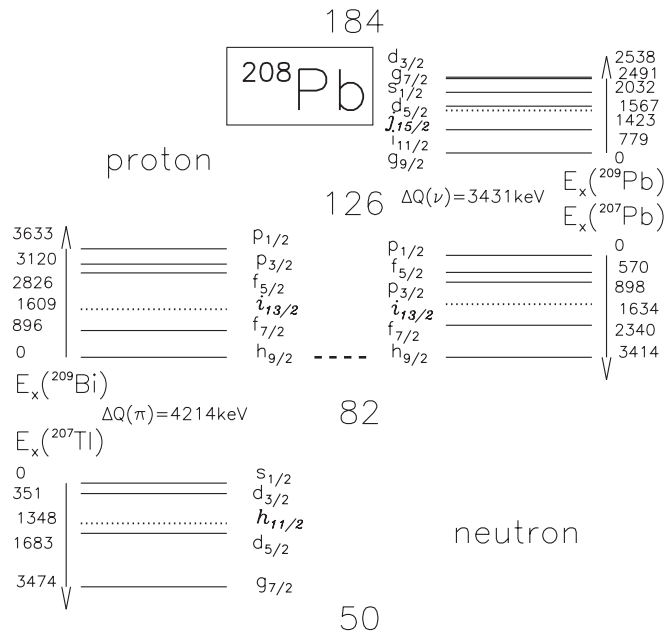

FIG. 1. Excitation energies in ^{208}Pb, ^{207}Pb, ^{209}Bi, ^{207}Tl determined from experiment [15] and gaps ΔQ derived from mass differences [Eq. (2)]. The magic gaps at 50, 82, 126, 184 nucleons, and the intruder levels (dotted, italic) are indicated. The $h_{9/2}$ orbits for protons and neutrons are matched to each other.

where one of the nucleons is an intruder (dotted lines). For more than 30 states, spectroscopic information about the configurations $j_{15/2}\, lj, lj = p_{1/2}, f_{5/2}, p_{3/2}$, is obtained from the experiment.

An essential part of the Coulomb pairing energy ΔE_C [Eq. (1)] derives from the nonlinear increase of the binding energy with neutron number N and proton number Z, see Eq. (2-19) in [19]. We use the values $\Delta E_C(A, N) = 0$ MeV, $\Delta E_C(A, Z) = -0.30$ MeV.

Table I shows the excitation energies [Eq. (1)] calculated for positive parity states with $E_x < 6.9$ MeV. Only the multiplets $j_{15/2}\, lj, lj = p_{1/2}, f_{5/2}, p_{3/2}$, are completely shown; for some other configurations more spins are predicted. For $6.2 < E_x < 6.6$ MeV a large gap is expected.

2. More-particle more-hole configurations

For the positive parity states the opportunity is given to determine the mixing between 1p-1h and 2p-2h configurations. Namely the lowest $15/2^-$ state in ^{208}Pb is no pure single particle state and hence all particle-hole configurations built in the proton decay of the $j_{15/2}$ IAR are already mixtures of 1p-1h and 2p-2h configurations. The lowest $9/2^+$ and $15/2^-$ states in ^{209}Pb are described by Bohr and Mottelson [20] as

$$\begin{aligned} |\hat{g}_{9/2}\rangle &= 0.97|0^+\text{g.s.} \otimes g_{9/2}\rangle + 0.24|2614\ 3^- \otimes j_{15/2}\rangle, \\ |\hat{j}_{15/2}\rangle &= 0.85|0^+\text{g.s.} \otimes j_{15/2}\rangle + 0.52|2614\ 3^- \otimes g_{9/2}\rangle. \end{aligned} \tag{3}$$

The states $\hat{g}_{9/2}$, $\hat{j}_{15/2}$ in ^{209}Pb may be considered as generalized particles similar to the more complicated situation in the $N = 82$ nuclei [8,21]. So in the following, by simply writing $g_{9/2}$, $j_{15/2}$ instead of $\hat{g}_{9/2}$, $\hat{j}_{15/2}$, we always have the structure

TABLE I. For spins 5^+–10^+ and $E_x < 6.9$ MeV in ^{208}Pb, shell model excitation energies $E_x^{\rm SSM}$ calculated by Eq. (1). Each configuration is given an order number n. For spin 6^+ an additional 2p-2h configuration is expected at $E_x \approx 5.2$ MeV (Sec. II A). IAR-pp' may determine amplitudes of the configurations $j_{15/2}p_{1/2}$, $j_{15/2}f_{5/2}$, $j_{15/2}p_{3/2}$.

Particle-hole configuration	$E_x^{\rm SSM}$ MeV	I_n^π					
		5^+	6^+	7^+	8^+	9^+	10^+
$\nu\ \boldsymbol{j_{15/2}\ p_{1/2}}$	4.854			1	1		
$\nu\ g_{9/2}\ i_{13/2}$	5.064	1	1	2	2	1	1
$\pi\ h_{9/2}\ h_{11/2}$	5.262	2	2	3	3	2	2
$\nu\ \boldsymbol{j_{15/2}\ f_{5/2}}$	5.424	3	3	4	4	3	3
$\pi\ i_{13/2}\ s_{1/2}$	5.522		4	5			
$\nu\ \boldsymbol{j_{15/2}\ p_{3/2}}$	5.752		5	6	5	4	
$\nu\ i_{11/2}\ i_{13/2}$	5.843	4	6	7	6	5	4
$\pi\ i_{13/2}\ d_{3/2}$	5.873	5	7	8	7		
$\pi\ f_{7/2}\ h_{11/2}$	6.159	6	8	9	8	6	
$\pi\ d_{5/2}\ i_{13/2}$	6.631	7	9	10	9	7	

of Eq. (3) in mind. The neutron holes just couple to these configurations.

Yet the states with spin 6^+ excited by IAR-pp' via the $j_{15/2}$ IAR through the configurations $j_{15/2}f_{5/2}$ and $j_{15/2}p_{3/2}$ contain also admixtures of the double-octupole configuration $|2614\ 3^-\rangle \otimes |2614\ 3^-\rangle$ [22–24].

The challenge to the experimentalist is the need to detect at least eight 6^+ states below $E_x = 6.1$ MeV and to determine the main configurations for each of them. From the recent compilation by NDS2007, four 6^+ states are assigned. Three assignments are confirmed, another one is shown to belong to a different member of a 5 keV doublet. From the tentative assignment of two more 6^+ states by NDS2007, one is confirmed, the other assignment indicates the problem of determining the L-value from high-energy ^{208}Pb(p,p') [25], see Secs. III, III D, IV F. We identify two more 6^+ states.

In ^{209}Pb, the lowest negative parity states start shortly above the fourth positive parity state ($s_{1/2}$, $E_x = 2.0$ MeV) [26–28]. They are described by configurations such as $g_{9/2}{}^2 p_{1/2}{}^{-1}$, $g_{9/2}{}^2 f_{5/2}{}^{-1}$. Hence their coupling with a $p_{1/2}$, $f_{5/2}$, $p_{3/2}$ hole yields positive parity states in ^{208}Pb with low spin. The IAR of these negative parity states above $E_p = 17.0$ MeV in ^{209}Bi are expected to be weak because of the multiparticle structure. The excitation functions covering the region above the $s_{1/2}$ IAR do not indicate an excitation of positive parity states with cross sections larger than 5 μb/sr which is neither explained by identified states, nor by states with large direct-pp' contributions or doublets. However only few proton energies were used to cover the excitation functions in this region.

The next $\frac{15}{2}^-$ state in ^{209}Pb (with a structure complementary to the lowest $\hat{j}_{15/2}$ state [Eq. (3)]) is suggested at $E_x = 3.05$ MeV [27,28]. The coupling of a $p_{1/2}$, $f_{5/2}$, $p_{3/2}$ hole to this state yields states in ^{208}Pb at $E_x \approx 7.0$ MeV, far above the region of $4.5 < E_x < 6.1$ MeV where the lowest positive parity states with spins 5^+–10^+ are expected (Table I).

In this paper the (generalized) 1p-1h frame seems acceptable for the discussion of the configurations $j_{15/2}p_{1/2}$, $j_{15/2}f_{5/2}$, $j_{15/2}p_{3/2}$ determined in states with excitation energies of $4.5 < E_x < 6.1$ MeV. For the 6^+ states an admixture from 2p-2h configurations should be considered, but is ignored in this paper, since we identify less states than predicted by the SSM.

B. Description of states

A particle-hole state with energy label E, spin I, parity π is described by a superposition of particle-hole configurations built from neutrons (ν) and protons (π) relative to the 0^+ ground state (g.s.) of ^{208}Pb with amplitudes c,

$$|E, I^\pi, M\rangle = \sum_{LJ}\sum_{lj} c^{E\,I^\pi,\nu}_{LJ,lj}\,|(\nu, LJ\otimes\nu, lj)I, M\rangle + \sum_{LJ}\sum_{lj} c^{E\,I^\pi,\pi}_{LJ,lj}\,|(\pi, LJ\otimes\pi, lj)I, M\rangle, \quad (4)$$
$$M = -I, \ldots, +I.$$

In a short-hand notation the state is described by

$$EI^\pi \equiv |E, I^\pi, M\rangle \text{ for any magnetic substate } M. \quad (5)$$

The particles are characterized by their angular momentum L and spin J, the holes similarly by l, j. The energy label E is defined by the excitation energy of the state (given by NDS2007 unless the state is new) rounded to keV. In order to achieve an unique energy label, sometimes 1 keV is added or subtracted.

By ordering the configurations according to their excitation energy, an order number n of the configuration is defined. So I_n^π may be written instead of $|(LJ\,lj)_{I^\pi}\rangle$, see Table I. Similarly, in case a complete sequence of states with a certain spin, parity, and a dominant configuration as expected from the SSM is identified, we simply write I_N^π, $N = 1, 2, \ldots$. In some cases a state number out of the complete sequence is tentatively designed as $I_{(N)}^\pi$ with N being the order number of the SSM configuration, if states with intermediate numbers may be expected but are not yet identified. For the 6^+ states order numbers $N > 2$ are set into parentheses, see Sec. II A.

C. Principles of the IAR-pp' reaction

The theoretical description of IAR-pp' is valid for isolated IAR [5,8]. The IAR $j_{15/2}$ in ^{209}Bi as the intruder is best isolated among all IAR. The next IAR of the same parity is expected near $E_p = 18.0$ MeV (Sec. II A).

1. *Isobaric analog resonances*

The wave function of a single particle (s.p.) IAR in ^{209}Bi with spin LJ may be represented by

$$\left|\Psi^{\rm IAR}_{LJ}(^{209}{\rm Bi})\right\rangle = \frac{1}{\sqrt{2T_0+1}}\,T_-(|LJ,\nu\rangle \otimes |^{208}{\rm Pb}(0^+\ {\rm g.s.})\rangle), \quad (6)$$

where $T_0 = \frac{N-Z}{2} = \frac{44}{2}$ is the isospin of the g.s. of ^{208}Pb. The isospin lowering operator T_- acts on all excess neutrons. In

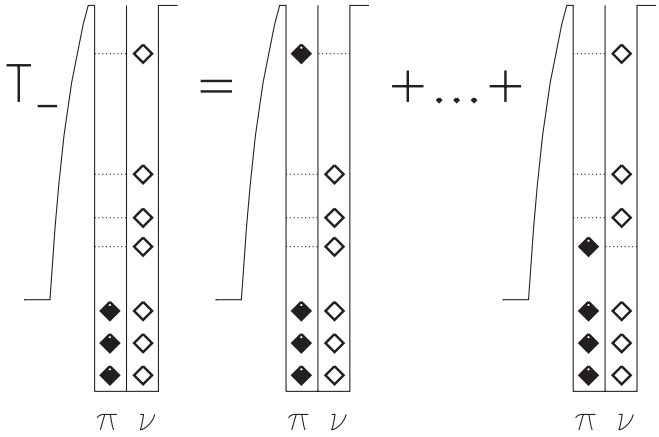

FIG. 2. Action of the isospin lowering operator T_- on the excess neutrons in ^{209}Pb [Eqs. (6), (7)] where $T_0 = \frac{44}{2}$ creates 45 components of the IAR. In each component one neutron (ν) is converted into a proton (π). However only six out of the 164 core nucleons ($N, Z \leqslant 82$), three out of the 44 excess neutrons ($82 < N, Z \leqslant 126$), and one orbit above $N, Z = 126$ are shown. The depicted Coulomb barrier explains the change of the penetrability with the proton energy [7].

each of the 45 components, one excess neutron is converted into a proton,

$$\left|\Psi_{LJ}^{\mathrm{IAR}}(^{209}\mathrm{Bi})\right\rangle = \frac{1}{\sqrt{2T_0+1}}|LJ,\pi\rangle \otimes |^{208}\mathrm{Pb}(0^+\ \mathrm{g.s.})\rangle + \sum_{lj}\sqrt{\frac{2j+1}{2T_0+1}}(|lj^{+1},\pi\rangle \otimes |lj^{-1},\nu\rangle)_{0^+} \otimes |LJ,\nu\rangle \otimes |^{208}\mathrm{Pb}(0^+\ \mathrm{g.s.})\rangle. \quad (7)$$

Figure 2 shows the action of the isospin lowering operator. The IAR consists of $2T_0 + 1$ configurations where either a proton is coupled to the parent nucleus (middle frame) or a neutron is coupled to the parent nucleus **and** one excess neutron in the parent nucleus is converted into a proton (right frame).

In the proton decay of the IAR either the proton escapes with the unchanged energy E_p (elastic proton scattering) and leaves ^{208}Pb in its g.s. (left frame of Fig. 3) or the proton escapes with the energy $E_{p'} = E_p - E_x$ (*in*elastic proton scattering) and excites neutron particle-hole configurations in the parent nucleus with the energy E_x (right frame of Fig. 3).

In contrast to the equivalent pickup reaction ^{209}Pb$^*(p,d)$, inelastic proton scattering via the IAR LJ creates a superposition of neutron particle-hole configurations $LJ\,lj$ in the parent nucleus. Hence the angular distribution is affected by the interference between all components and the *amplitude* $c_{LJ,lj}^{E\,I^\pi,\nu}$ of each configuration $LJ\,lj$ including the sign can be determined [Eq. (4)].

2. *Cross section of IAR-pp′*

The differential cross section is described by a product of four factors [5,8].

(i) One factor describes the population of the IAR with orbital momentum L and spin J as a function of the s.p. width $\Gamma_{LJ}^{\mathrm{s.p.}}$, the total width $\Gamma_{LJ}^{\mathrm{tot}}$ and the resonance energy E_{LJ}^{res}.

(ii) A second factor describes the decay of the IAR given by the s.p. width $\Gamma_{lj}^{\mathrm{s.p.}}$ and the phase between the interfering amplitudes of the decaying particles with orbital momentum l and spin j.

(iii) A third factor describes the geometry of the angular momenta L, l and spins J, j recoupling to the final spin I.

(iv) A fourth factor describes the resonance behavior. The pattern of the excitation function is described to first order [4,5] by a Lorentzian shape,

$$R^{\mathrm{res}}(E_p, LJ) = \frac{{\Gamma_{LJ}^{\mathrm{tot}}}^2}{4\left(E_p - E_{LJ}^{\mathrm{res}}\right)^2 + {\Gamma_{LJ}^{\mathrm{tot}}}^2}. \quad (8)$$

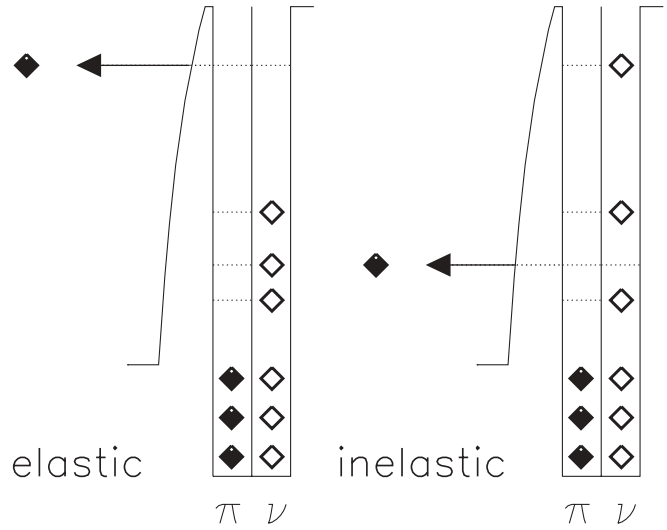

FIG. 3. The proton decay of an IAR. The left frame reflects the elastic proton scattering, the right frame the *in*elastic proton scattering creating neutron particle-hole configurations in the parent nucleus.

Both the incoming and outgoing particles have to overcome the Coulomb barrier of the nucleus (see Figs. 2, 3). The penetrability of the escaping proton strongly increases with proton energy E_p and is much lower for protons with higher angular momentum L or l [7], see also Table II. Therefore an asymmetric pattern of the excitation function is expected which indeed is already observed in the very first experiments on ^{208}Pb(p,p') via IAR in ^{209}Bi [3]. It has been described by different formulas [4,5].

Table II shows relevant IAR parameters.

For a pure configuration $LJ\,lj$ the shape of an angular distribution is given by geometrical factors only, a product of $3j$ and $6j$ symbols [5]. In general however, the shape of the angular distribution is distorted by the configuration mixing (see, e.g., [2,8]).

Only for the 5615, 5742, 5764 states, the shape of the angular distribution is discussed in this work. In order not to lengthen the paper, we otherwise discuss only mean cross sections, no details of angular distributions.

The measured angular distributions for ^{208}Pb(p,p') via IAR in ^{209}Bi can be fitted by a series of even order Legendre

TABLE II. Parameters for IAR in ^{209}Bi.

IAR LJ	E_{LJ}^{res} [a] MeV [4]	$\Gamma_{LJ}^{\mathrm{tot}}$ keV [4]	$\Gamma_{LJ}^{\mathrm{s.p.}}$ [b] keV [5]
$g_{9/2}$	14.918 ± 0.006	253 ± 10	20 ± 1
$i_{11/2}$	15.716 ± 0.010	224 ± 20	2.2 ± 0.3
$j_{15/2}$ [c]	16.375 ± 0.010	210 ± 10	0.8 ± 0.1
$d_{5/2}$ [d]	16.496 ± 0.008	308 ± 8	45 ± 5
$s_{1/2}$	16.965 ± 0.014	319 ± 15	45 ± 8
$g_{7/2}$	17.430 ± 0.010	288 ± 20	45 ± 10
$d_{3/2}$	17.476 ± 0.010	279 ± 20	35 ± 10
Hole lj	$E_{p'}^{\mathrm{SSM}}(LJ\,lj)$ [e] MeV		$\Gamma_{lj}^{\mathrm{s.p.}}$ [5] keV
$p_{1/2}$	11.49		28.6 [f]
$f_{5/2}$	10.92		5.2 ± 0.4
$p_{3/2}$	10.59		14.6 ± 0.5
$i_{13/2}$	9.86		0.06 [g]
$f_{7/2}$	9.15		0.67 ± 0.04 [h]
$h_{9/2}$	8.08		0.04 [g]

[a] Resonance energy in the laboratory system.
[b] The uncertainties for the $g_{9/2}$, $d_{5/2}$, $s_{1/2}$, $g_{7/2}$, $d_{3/2}$ IAR may be larger than estimated from [4].
[c] Values determined by this work.
[d] $E_{d_{5/2}}^{\mathrm{res}}$ taken as reference value (Sec. III F). In this paper $\Gamma_{LJ}^{\mathrm{tot}} = 300$ keV is used.
[e] $E_{p'}^{\mathrm{SSM}}(LJ\,lj) = E_{LJ}^{\mathrm{res}} - E_x^{\mathrm{SSM}}(LJ\,lj)$, see Eq. (1).
[f] Reference value from [4], see also [5].
[g] Calculated [7].
[h] From [29].

polynomials P_K,

$$\frac{d\sigma}{d\Omega}(E, I^\pi, \Theta, E_p) = \sum_{K=\mathrm{even}} A_K(E, I^\pi, E_p) P_K(\cos\Theta). \quad (9)$$

The mean cross section is described by the isotropic component,

$$\sigma^{\mathrm{mean}}(E, I^\pi, E_p) = A_0(E, I^\pi, E_p). \quad (10)$$

We define the angle integrated cross section

$$\sigma^{\mathrm{avg}}(E, I^\pi, E_p) = \frac{1}{n}\sum_{i=1}^{n} \frac{d\sigma}{d\Omega}(E, I^\pi, \Theta^i, E_p) \quad (11)$$

as an acceptable approximation of the mean cross section σ^{mean} [Eq. (10)] but systematically different from it. Namely the shape of the angular distribution is often pronounced and the measured data points do not cover the full range of scattering angles sufficiently well.

The excitation of a state by the intruder IAR $j_{15/2}$ assigns positive parity. Because of the often pronounced angular distribution, the measurement of excitation functions should be done for a certain scattering angle. However, because of the limited amount of data, we compare differential cross sections [Eq. (9)] determined for some *range* of scattering angles $\tilde{\Theta}$ and for some *range* of bombarding energies $\tilde{E}_p$ relative to the $j_{15/2}$ IAR,

$$R_{j_{15/2}}^{\mathrm{avg}}(E, I^\pi, \tilde{E}_p) = \frac{1}{m}\sum_{i=1}^{m}\frac{1}{n}\sum_{k=1}^{n} \frac{\frac{d\sigma}{d\Omega}\left(E, I^\pi, \Theta^i, E_p^k\right)}{\frac{d\sigma}{d\Omega}\left(E, I^\pi, \Theta^i, E_{j_{15/2}}^{\mathrm{res}}\right)},$$
$$\tilde{\Theta} = \frac{1}{m}\sum_{i=1}^{m}\Theta^i \approx 90^\circ, \quad \tilde{E}_p = \frac{1}{n}\sum_{k=1}^{n} E_p^k. \quad (12)$$

D. ^{207}Pb(d,p), ^{209}Bi(d,He)

By using the Q3D magnetic spectrograph at München, the reaction ^{207}Pb(d,p) was measured at scattering angles $\Theta = 20^\circ, 25^\circ, 30^\circ$ for $3.1 < E_x < 8.0$ MeV [5].

For all states in Table III excited by ^{207}Pb(d,p) a mean cross section is determined,

$$\sigma_{(d,p)}^{\mathrm{avg}}(E, I^\pi) = \frac{1}{3}\sum_{\Theta=20^\circ,25^\circ,30^\circ} \frac{d\sigma_{(d,p)}}{d\Omega}(E, I^\pi, \Theta). \quad (13)$$

The strength c^2 [Eqs. (4), (5), Table IV] for the configurations $LJ\ p_{1/2}$ is derived from the spectroscopic factors [12]. By comparison to DWBA calculations configuration strengths for more states are derived from the mean cross sections $\sigma_{(d,p)}^{\mathrm{avg}}$ obtained by this work.

By chance for $\Theta = 20^\circ, 25^\circ, 30^\circ$ the slope of the angular distribution for $l = 0$ and $l = 7$ is steep in contrast to rather flat angular distributions for other l values. In Table III l values derived from this work are given in parentheses.

Table III shows spectroscopic factors C^2S from ^{209}Bi(d,^{3}He) [30] and S_{rel} from ^{209}Bi(t, $\alpha\,\gamma$) [31]. For several states upper limits of spectroscopic factors for $h_{9/2}h_{11/2}$ are determined by recalibration of a few spectra [32].

III. EXPERIMENTAL DATA

We evaluate data taken with the Q3D magnetic spectrograph of the Maier-Leibnitz-Laboratorium at the München 14 MV tandem accelerator for ^{207}Pb(d,p) [5] and since 2003 for ^{208}Pb(p,p') via IAR in ^{209}Bi. More literature data are considered [6].

Within $L \pm \delta L$, $\delta L \leqslant 1$, the angular momentum L determined from ^{208}Pb(p,p') at $E_p = 35$ MeV [25] (with a resolution of about 7 keV) is accepted if the level is resolved.

Experimental data are shown in Table III. For positive parity states in close doublets, data for the neighboring states are included. Also included is the 5690 4^+ state which is excited by direct-pp' with a mean cross section $\sigma^{\mathrm{avg}} = 7$–$20\,\mu$b/sr increasing linearly for $E_p = 14.8$–18.1 MeV. In addition the 5260, 5958 states are included, see Sec. IV H.

The dominant configuration is suggested by comparison to the SSM. For states strongly excited in the $j_{15/2}$ IAR with excitation energies $4.6 \lesssim E_x \lesssim 4.9$, $4.9 \lesssim E_x \lesssim 5.6$, $5.6 \lesssim E_x \lesssim 6.1$ MeV, the configuration $j_{15/2}p_{1/2}$, $j_{15/2}f_{5/2}$, $j_{15/2}p_{3/2}$ is expected, respectively (Table I).

TABLE III. Excitation energy, spin I, and parity π of states in ^{208}Pb for $E_x < 6.0$ MeV assumed to have positive parity [6] and identified by this work [^{208}Pb(p,p') , ^{207}Pb(d,p)]. Other states from doublets (Sec. III D) are included. L values from ^{208}Pb(p,p') [25], spectroscopic factors C^2S from ^{209}Bi$(d,^3$He) [30], and relative spectroscopic factors $S_{\rm rel}$ from ^{209}Bi$(t,\alpha\gamma)$ [31] are included.

Fig.[l]	E	Excitation energy			$\sigma^{\rm avg}$		l	I	π	Main	I^π	L	C^2S[o]	$S_{\rm rel}$
		keV	(p,p') keV	(d,p) keV	on $j_{15/2}$[m] μb/sr	(d,p)[m] μb/sr	(d,p)[n]			p-h config.		(p,p')		
		[6]	–	this	– –	– –	– –	work		–	[6]	[25]	[30]	[31]
	4424	4423.647 ± 0.015	4423.7 ± 0.4	4423.4 ± 0.7	26 ± 5	0.3 ± 1		6	+	$g_{9/2}i_{13/2}$	6^+	6	0.27	1.28
	4611	4610.748 ± 0.016	4610.7 ± 0.3	4610.5 ± 0.2	18 ± 2	7.0 ± 5	7	8	+	$j_{15/2}p_{1/2}$	8^+	8	0.19	1.31
6	4861	4860.78 ± 0.06	4860.7 ± 0.3	4860.8 ± 0.3	11 ± 2	3.0 ± 3	7	8	+	$g_{9/2}i_{13/2}$	8^+	[a]	0.25	1.62
6	4868	4867.91 ± 0.04	4867.8 ± 0.2	4867.9 ± 0.2	25 ± 2	10.0 ± 8	7	7	+	$j_{15/2}p_{1/2}$	7^+	[a]	<0.1	
6	4895	4895.23 ± 0.05	4895.0 ± 0.8		1.0 ± 0.3	<0.1		10	+	$g_{9/2}i_{13/2}$	10^+	≈10	0.61	3.32
	4928	4928.1 ± 1.5	4929.0 ± 0.4		(3) ± 1.0	<0.1		2	+		2^+		<0.1	
6, 7	4929		[b]		[b]	[b]		5	+	$g_{9/2}i_{13/2}$		4	<0.1	
7	4995	4994.7 ± 0.6	4993.7 ± 0.8	4995 ± 1	2.0 ± 1.5	<1.5		7	+	$g_{9/2}i_{13/2}$		⩾8	<0.1	
7	5010	5010.43 ± 0.14	5010.6 ± 0.8		1.5 ± 0.8	<0.1		9	+	$g_{9/2}i_{13/2}$	9^+	9	<0.1	0.30
7	5069	5069.31 ± 0.10	5069.1 ± 0.7	5068.7 ± 0.9	1.7 ± 0.5	<0.2		10	+	$h_{9/2}h_{11/2}$	10^+	(9)	0.74	3.22
7	5093	5092.99 ± 0.03	5093.3 ± 0.5	5093.4 ± 0.4	5.0 ± 0.5	0.6 ± 0.2	(7)	8	+	$h_{9/2}h_{11/2}$	8^+		0.21	1.99
	5162	5162.05 ± 0.05	5162.4 ± 0.9		1.3 ± 0.5	<0.1		9	+	$h_{9/2}h_{11/2}$	9^+	[c]	1.71	9.76
	5193	5193.428 ± 0.025			<0.5			5	+	$h_{9/2}h_{11/2}$	5^+	[d]	1.86	4.83
	5194	5195.054 ± 0.023	[b]	5195.1 ± 0.4	(5) ± 1	(1.5) ± 0.3		3, 4	–		$3^-, 4^-$	[d]	[e]	[f]
	5195	5195.37 ± 0.10	5194.8 ± 0.4		[b]	[b]		7	+	$h_{9/2}h_{11/2}$	7^+	[d]	[e]	6.20
	5213	5213.007 ± 0.021	5214.1 ± 0.3		[b]			6	+	$h_{9/2}h_{11/2}$	6^+		1.17	4.63
	5214	5213.98 ± 0.03	[b]	5214.1 ± 0.1	(8) ± 1	(5.0) ± 5		2–5	–		(5^-)		[e]	[f]
	5216	5216.214 ± 0.018	[b]		[b]						4^+		[e]	1.32
	5260	5260 ± (6)[g]	[h]								9^+			
4	5326	5326.6 ± 0.2	5326.4 ± 0.3		6.5 ± 0.5	<0.1		9	+	$j_{15/2}f_{5/2}$	$^+$		<0.2	
4	5339	5339.46 ± 0.06	5339.4 ± 0.5		4 ± 1	<0.1		8	+	$j_{15/2}f_{5/2}$	8^+		0.52	2.54
4	5374	5373.8 ± 0.8	5373.5 ± 0.5	5373.6 ± 0.5	6.5 ± 0.5	0.3 ± 1	(7)	7	+	$j_{15/2}f_{5/2}$	$(6)^+$	5	<0.2	
4	5417	5418.6 ± 0.5	5418.6 ± 0.5		5 ± 1	<0.1		6	+	$j_{15/2}f_{5/2}$	$(6)^+$	[i]	<0.1	
	5537	5536.58 ± 0.19	5536.3 ± 0.5		4.5 ± 1.0	<0.1		10	+	$j_{15/2}f_{5/2}$	10^+		0.54	1.65
	5588	5587.7 ± 0.5	5587.6 ± 0.7		2.5 ± 0.5	<0.2		(5)	+	$j_{15/2}f_{5/2}$			<0.1	
	5615	5615.4 ± 0.4	5614.8 ± 0.2		17 ± 2	<0.1		7	+	$j_{15/2}p_{3/2}$	7^+	⩾6	<0.1	
4, 8	5640	5639.55 ± 0.09	5639.3 ± 0.8	5639.8 ± 0.3	[b]	[b]					1^-			
	5642	5641.98 ± 0.20	5641.9 ± 0.6		[b]	[b]					$1, 2^+$			
	5643	5643 ± 4	5642.8 ± 0.3		[b]	[b]		2–5	–		$2-7^-$			
	5648	5649.01 ± 0.06	5648.9 ± 0.3	5648.7 ± 0.6	[b]	(2.0) ± 0.2		2–5	–		$3^-, 4^-$		[j]	[j]
4, 8	5649	5649.5 ± 0.4	5649.4 ± 0.3		(13) ± 1	[b]		(9)	+	$j_{15/2}p_{3/2}$	$6-9^+$		[e]	[f]
5	5742	5741.1 ± 0.4	5741.7 ± 0.3	5741.5 ± 0.4	11.5 ± 1.0	0.5 ± 2	(7)	8	+	$j_{15/2}p_{3/2}$	$6-9^+$	9	<0.1	
5	5764	5763.7 ± 0.8	5764.1 ± 0.6		3.5 ± 0.5	<0.1		6	+	$j_{15/2}p_{3/2}$	6^+	6	<0.1	
5, 9	5899	5901 ± 3	5899.2 ± 0.4		5.0 ± 0.5	<0.1		(9)	+	$i_{11/2}i_{13/2}$	$(8)^+$	(8)	<0.2	
	5928	5928.0 ± 0.3	5927.4 ± 0.9		<0.5	<0.1		10	+	$i_{11/2}i_{13/2}$	10^+		0.29	1.59
	5958	5954 ± 6	5957.6 ± 1.0		1.0 ± 0.8	<0.1		(9)	+	$(f_{7/2}h_{11/2})$	9^+		<0.1	
9	5989	5989.1 ± 1.2	5988.7 ± 0.9		1.5 ± 0.8	<0.1		6	+	$i_{13/2}d_{3/2}$		[k]	<0.1	
	5993	5992.67 ± 0.25	5994.3 ± 0.5		(25) ± 5[a]	<0.1		2–5	–		6^+	[k]		

[a] Doublet structure.
[b] Doublet discussed in Sec. III D.
[c] Level seen, but no L-value given.
[d] $L = 3$ for apparently dominant member.
[e] Doublet not resolved [30].
[f] Doublet not resolved [31].
[g] Uncertainty not given [6].
[h] See Sec. IV H.
[i] $L = 6$ or $L = 7$, probable doublet structure.
[j] $h_{9/2}d_{5/2}$ [30,31].
[k] $L = 6$ for $E_x = 5.993 \pm 0.003$ MeV.
[l] Level shown in the given figure.
[m] Values in parentheses for doublets.
[n] Values in parentheses from this work; others from [12].
[o] U.L. for $h_{9/2}h_{11/2}$ from this work [32].

TABLE IV. (Columns 1–2) Identified states with spins 5^+–10^+. Spin and parity assignments I^π from NDS2007 are marked in bold. The order number N is explained in Sec. II B. (Column 3) Mean cross section $\sigma^{\rm avg}$ from IAR-pp' (Sec. III E). Values for members of doublets are given in parentheses (Sec. III D). (Column 4) Configuration strength c^2 [Eq. (4)] for $j_{15/2}p_{1/2}$ derived from spectroscopic factors [12]. Upper limits and values in parentheses are obtained by this work. (Columns 5–12) Excitation functions given by the ratio of mean cross sections $R^{\rm avg}{}_{j_{15/2}}$ [Eq. (12)] for $E_p = 14.92$–17.50 MeV corresponding to the $g_{9/2}$, $i_{11/2}$, $j_{15/2}$, $d_{5/2}$, $s_{1/2}$ IAR and the $g_{7/2}$, $d_{3/2}$ doublet IAR and two more proton energies near the $j_{15/2}$, $d_{5/2}$ IAR.

	E	I^π_N	$\sigma^{\rm avg}$	c^2	$R^{\rm avg}{}_{j_{15/2}}(E, I^\pi, \tilde{E}_p)$							
			[Eq. (11)]	from	$g_{9/2}$	$i_{11/2}$	$j_{15/2}$		$d_{5/2}$		$s_{1/2}$	$g_{7/2}+d_{3/2}$
			μb/sr	^{207}Pb(d,p) [12]	14.92 MeV	15.72 MeV	16.29 MeV	16.40 MeV	16.50 MeV	16.62 MeV	16.96 MeV	17.50 MeV
[a]	4929[b]	$(5_1)^+$	3.0		0.4	0.2	0.5	1 ± 0.4	0.8	0.6	0.4	0.2
	5193	$\mathbf{5^+_2}$	<0.5					[c]				
[a]	5588	$(5_3)^+$	2.5		0.3	0.3	0.8	1 ± 0.3	0.7	0.5	0.6	0.7
	4424	$\mathbf{6^+_1}$	26.0					direct-pp' dominant				
	5213[b]	$\mathbf{6^+_2}$	(8)		0.9	0.5	0.8	1 ± 0.3	0.7	0.6	0.8	0.8
[a]	5417	$6^+_{(3)}$	6.5		0.2	0.2	0.8	1 ± 0.2	0.6	0.3	0.3	0.3
	5764	$\mathbf{6^+_{(5)}}$	3.5		0.3	0.2		1 ± 0.2	0.3	0.3	0.4	0.3
	5989	$\mathbf{6^+_{(7)}}$	1.5		0.5		0.8	1 ± 0.5	0.8	0.8		
[a]	4868	$\mathbf{7^+_1}$	24.0	0.90 ± 0.06	0.1	0.1	0.8	1 ± 0.2	0.4	0.2	0.2	0.2
	4995	$(7_2)^+$	1.5	<0.10	0.2		0.4	1 ± 0.7	0.8	0.6		
	5195[b]	$\mathbf{7^+_3}$	(5)	<0.03	0.3		0.7	1 ± 0.2	0.8		1.0	1.0
[a]	5374	7^+_4	6.5	(0.03 ± 0.01)	0.1	0.1	0.8	1 ± 0.2	0.5	0.2	0.3	0.3
[a]	5615	$\mathbf{7^+_{(6)}}$	17.0	<0.03	0.1	0.1	0.7	1 ± 0.1	0.5	0.3	0.2	0.3
[a]	4611	$\mathbf{8^+_1}$	18.0	0.63 ± 0.05	0.1	0.2	0.8	1 ± 0.1	0.7	0.5	0.6	0.6
[a]	4861	$\mathbf{8^+_2}$	10.0	0.27 ± 0.05	0.1	0.1	0.8	1 ± 0.2	0.6	0.5	0.3	0.3
[a]	5093	$\mathbf{8^+_3}$	5.0	(0.05 ± 0.02)	0.2	0.6	0.8	1 ± 0.1	0.5	0.5	0.2	
	5339	$\mathbf{8^+_4}$	4.0	<0.03	0.2	0.2	0.8	1 ± 0.3	0.6	0.2	0.5	0.6
[a]	5742	8^+_5	11.5	(0.05 ± 0.02)	0.1	0.1	0.8	1 ± 0.3	0.5	0.3	0.2	0.2
[a]	5010	$\mathbf{9^+_1}$	1.5		0.2		0.4	1 ± 0.6	0.7	0.7	0.4	
	5162	$\mathbf{9^+_2}$	1.3				0.6	1 ± 0.6	0.8		0.4	
[a]	5326	9^+_3	6.5		0.2	0.2	0.8	1 ± 0.2	0.5	0.2	0.4	0.2
	5649[b]	$(9_4)^+$	(13)		0.2	0.1	0.5	1 ± 0.5	1.1	0.8	0.3	0.2
	5900	$(9_5)^+$	4.0		0.3		0.6	1 ± 0.2	0.6	0.5	0.4	0.3
	5958	(9^+_6)	2.0					[d]				
	4895	$\mathbf{10^+_1}$	1.0			0.8	0.9	1 ± 0.5	0.9	0.9	0.9	0.9
	5069	$\mathbf{10^+_2}$	1.7		0.4		0.5	1 ± 0.4	0.6		0.6	0.7
[a]	5537	$\mathbf{10^+_3}$	4.5		0.1	0.2	0.8	1 ± 0.3	0.7	0.3	0.4	0.4
	5928	$\mathbf{10^+_4}$	<0.5					[c]				

[a]Excitation function shown in Figs. 10 and 11.
[b]Unresolved doublet (Sec. III D).
[c]No resonance seen.
[d]Section IV H.

A. Spectra

Survey spectra for IAR-pp' are shown in Figs. 4 and 5; spectra fitted by GASPAN are shown in Figs. 6–9. No scale for the ordinate is given, since the cross sections varies by a factor up to 5 for different scattering angles and by a factor up to 500 for different proton energies.

One spectrum of ^{208}Pb(p, p') taken with the Q3D magnetic spectrograph covers excitation energies corresponding to about 4% of the magnetic field, or $(E_x^{\rm max} - E_x^{\rm min})/(E_p - E_x^{\rm max}) \approx 0.08$. Hence at least three spectra have to be taken in order to cover the full range of interest $4.5 < E_x < 6.1$ MeV. In total more than 300 spectra taken at different scattering angles $20^\circ \leqslant \Theta \leqslant 138^\circ$, bombarding energies $14.8 < E_p < 18.1$ MeV and with several targets of 100–300 μg/cm^2 thickness are evaluated.

In Figs. 4 and 5 states with major fragments of the configurations $j_{15/2}f_{5/2}$, $j_{15/2}p_{3/2}$ are identified, see Table III. In Figs. 6–9 spin, state number, and parity from Tables III and IV—omitting the parentheses for tentative assignments—are given for positive parity states discussed in Secs. III D and IV.

The excitation energies in Figs. 6–9 differ from the values in Table III determined by Eq. (17), see Sec. III B2.

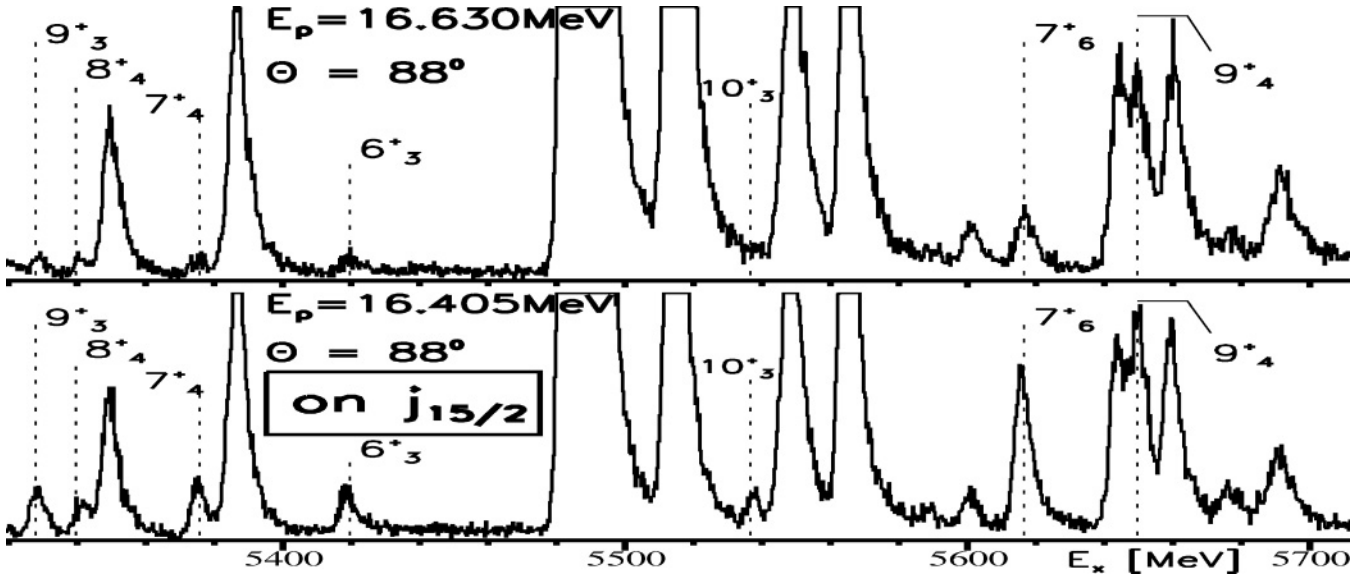

FIG. 4. Spectrum taken at scattering angle $\Theta = 88^\circ$ for $5.3 < E_x < 5.7$ MeV and proton energy $E_p = 16.630$ MeV (top: off resonance) and $E_p = 16.405$ MeV (bottom: on $j_{15/2}$ IAR). Some positive parity states are identified (dotted lines), see Tables III, IV. In the region $5.3 < E_x < 5.6$, $5.6 < E_x < 6.0$ the major fragments of the $j_{15/2} f_{5/2}$, $j_{15/2} p_{3/2}$ multiplet are located, respectively. The structure of other strongly excited states is not discussed.

B. Excitation energies

1. *Fit of spectra by* GASPAN

The determination of excitation energies from spectra taken with Q3D magnetic spectrograph of the Maier-Leibnitz-Laboratorium at München depends on the high linearity achieved with the present detector [11].

The fit of some spectrum by the computer code GASPAN [33] consists of the following steps:

(i) The spectrum is divided up into three to six parts because of the high level density. Gaps near deep minima or regions with broad contamination lines guide the divisions.

(ii) An automatic search at low sensitivity generates a list of peaks. From a crude energy calibration the biggest peaks are identified by comparison to NDS2007.

(iii) The width of the peaks is determined for strong peaks known from NDS2007 to belong to well isolated states. The width δ of each peak [Eq. (A1)] is fitted by

$$\delta(c) = \delta_0 + \delta_1 c, \tag{14}$$

where c is the channel number along the detector plane. A parabolic dependence similar to Eq. (15) has not to

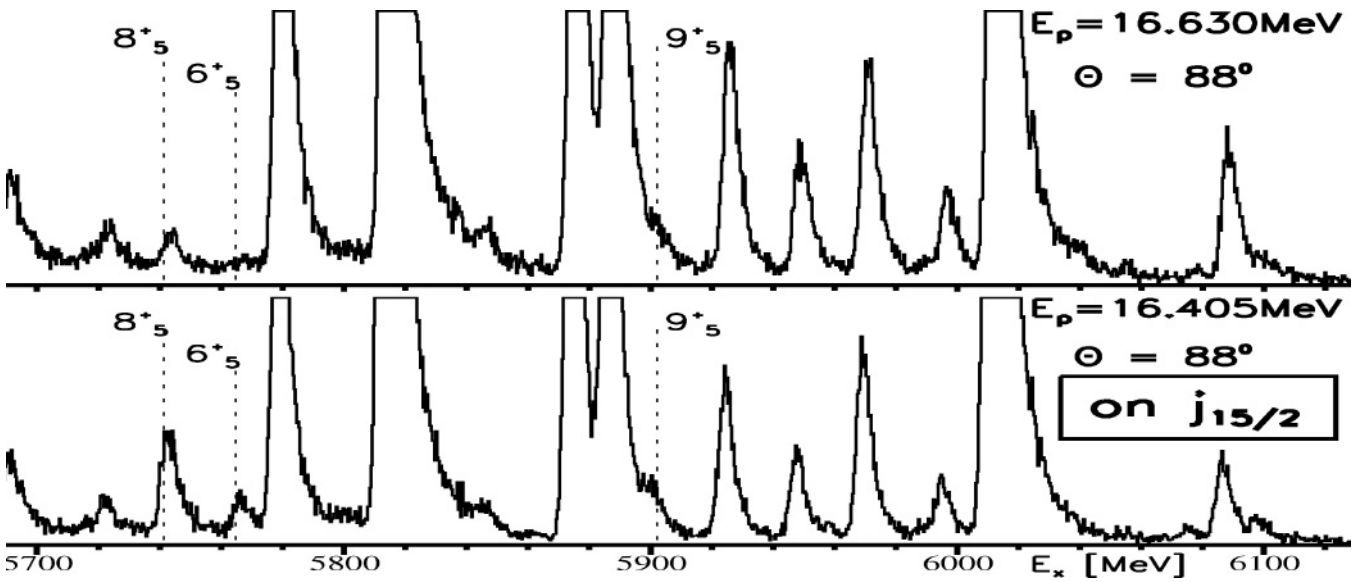

FIG. 5. Continuation of Fig. 4. Spectra taken for $5.7 < E_x < 6.1$ MeV.

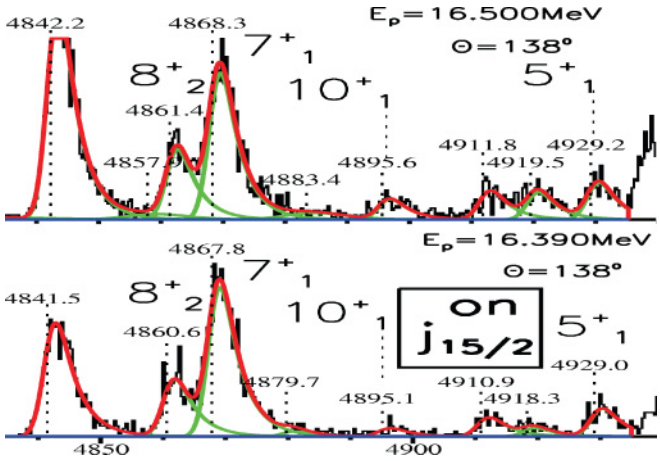

FIG. 6. (Color online) Spectra taken for $4.835 < E_x < 4.935$ MeV and fitted by GASPAN. Satellites from L electrons are fitted to the 4842, 4868 peaks (Appendix B).

be assumed, since each spectrum is fitted in separate parts with a length of $\Delta E_{p'}/\langle E_{p'}\rangle < 0.03$.

During this step contamination lines are fitted by broader lines or by adding a linear or a quadratic background (Appendix A). For some lines a significant deviation of the width from the mean value [Eq. (14)] reveals possible doublets.

(iv) Each peak is fitted by a Gaussian with an exponential tail [Eq. (A1)]. The width of the tail is determined on the side where $E_{p'} < E_p - E_x$.

(v) As explained in Appendix B, sometimes one or two secondary lines have to be added to strong peaks.

(vi) The quality of the fit by GASPAN is measured by the χ^2 criterion and by the spectrum of the residues from the fit [Eqs. (A4), (A5)]. Both criteria may reveal possible new levels or doublets.

(vii) In special cases new peaks are discovered by a GASPAN run minimizing the residue spectrum [Eqs. (A5), (A6)].

2. *Determination of excitation energies*

Each peak is fitted by a Gaussian of individual width and an exponential tail (Appendix A). In GASPAN spectra (Figs. 6–9), *the fitted value of the excitation energy is shown at the position of the Gaussian* [Eq. (A1)]. Because of the exponential tail the maximum is always at higher excitation energies. It does not matter since we always compare energy differences only [Eq. (17)].

The instrumental resolution is defined as the FWHM value of the peak given by the Gaussian proportional to δ [Eq. (A1)]. In the spectra only the half-width at the low excitation energy side assumes the value, while the *effective* half-width at the high excitation energy side is often much larger because of the tail. The intensity of the tail depends on the target thickness, the target angle, the scattering angle, the choice of backward or forward scattering and whether the carbon backing is crossed or not.

The precision of the excitation energies derived from the evaluation of the spectra by GASPAN is refined in an iterative manner of at least four main steps. In the first step

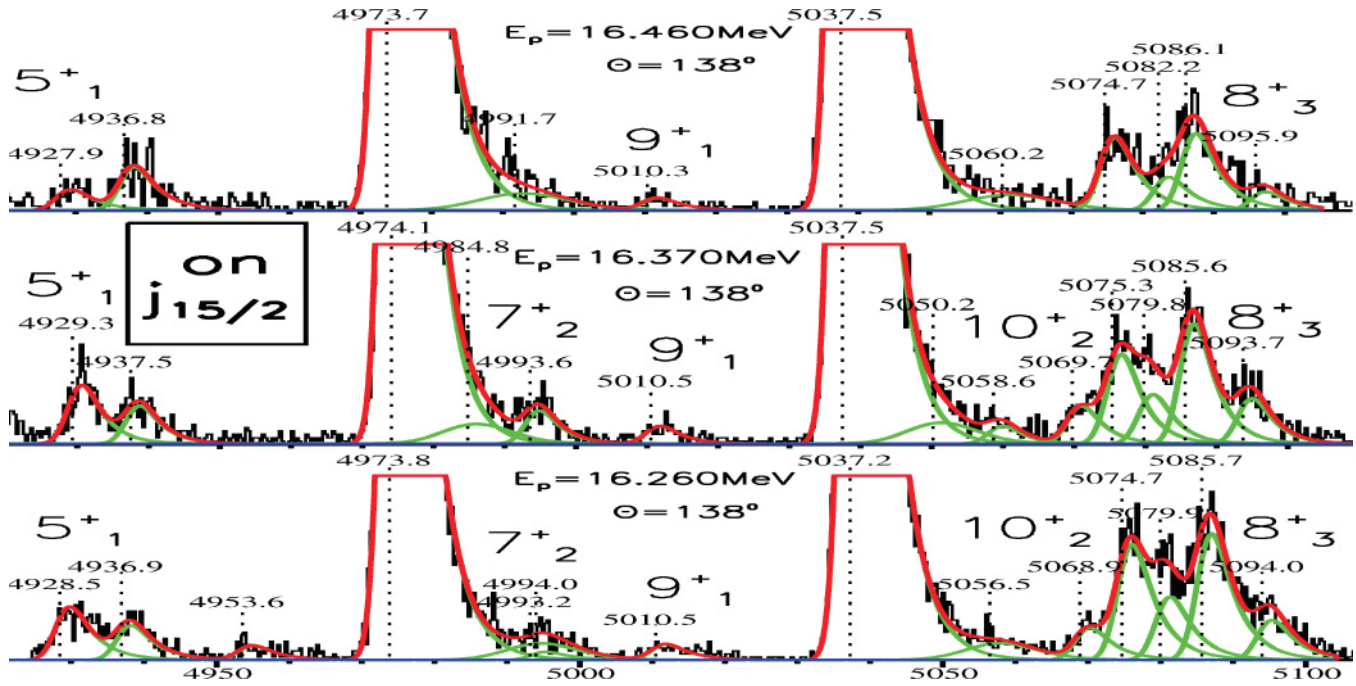

FIG. 7. (Color online) Spectra taken for $4.920 < E_x < 5.105$ MeV and fitted by GASPAN. The ratio of the 4929, 5010 peaks to the 4974 peak is about 4 : 100, 1 : 100, respectively. The cross sections for the 4974 and 5037 states are nearly equal and increase by a factor 2 from $E_p = 16.260$ to 16.460 MeV. Satellites from L electrons are fitted to the 4974 and 5037 peaks (Appendix B). In the lowest spectrum the proton energy is $E_p = 16.310$ MeV (not $E_p = 16.260$ MeV as indicated).

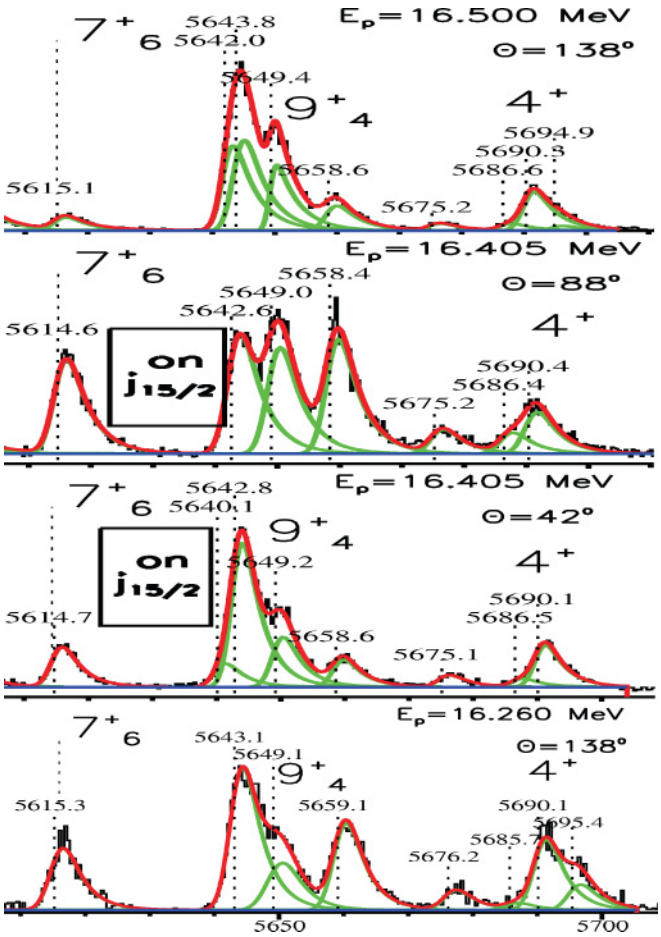

FIG. 8. (Color online) Spectra taken for $5.610 < E_x < 5.710$ MeV and fitted by GASPAN.

the proportionality of the magnetic field B to the energy of the scattered protons is used,

$$E_{p'}(c) = E_p - E_x^{\mathrm{GSP}}(c) = a_0 + a_1 c + a_2 c^2, \qquad (15)$$

where c is the channel number along the detector plane.

In a second step strong peaks are identified with known states by comparison to literature data [6] and the parameter set a_0, a_1, a_2 is improved.

By using another computer program, the congruence of the results for all runs (up to 200 runs for a certain region of excitation energies) is inspected and contamination lines from light nuclei or other lead isotopes are discriminated. New doublets and new states are investigated, too.

Another iteration with the GASPAN code [33] consists in the fit of many peaks known by NDS2007 to be no close doublets ($\delta E_x > 4$ keV). In this step the deviation of the excitation energy E_x^{GSP} [Eq. (15)] from E_x^{NDS} determined with high precision by γ spectroscopy [6] is fitted,

$$E_x^{\mathrm{GSP}}(c) = E_x^{\mathrm{NDS}}(c) + b_0 + b_1 c + b_2 c^2. \qquad (16)$$

From up to 200 different runs, a mean value of the energies $\langle E_x^{\mathrm{GSP}} \rangle$ is determined yielding the final value given in Table III,

$$\begin{aligned} E_x(c) &= E_x^{\mathrm{NDS}}(c) + \delta E'_x(c), \\ \delta E'_x(c) &= \left\langle E_x^{\mathrm{GSP}}(c) \right\rangle - E_x^{\mathrm{NDS}}(c) = c_0 + c_1 c + c_2 c^2. \end{aligned} \qquad (17)$$

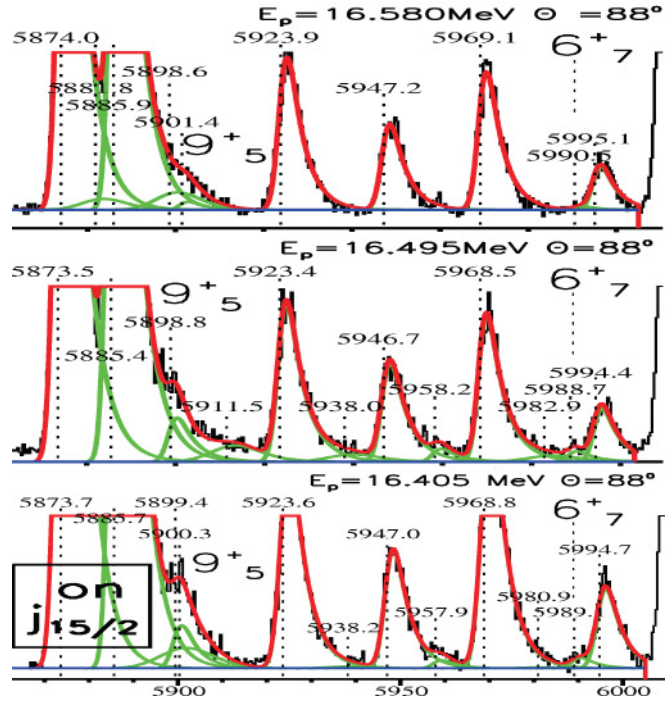

FIG. 9. (Color online) Spectra taken for $5.880 < E_x < 6.005$ MeV and fitted by GASPAN. Satellites from L electrons are fitted to the 5886, 5924, 5969 peaks (Appendix B).

The parameter c_0 is the mean deviation of all values E_x^{GSP} from the chosen excitation energies E_x^{NDS}. It should be small, $|c_0| \lesssim 1$ keV, and c_1, c_2 should nearly vanish, too, if the identification of *all known* levels with NDS2007 is correct and the statistics are high enough.

The parameters c_1, c_2 partially compensate for the nonlinear correction by the relativistic kinematics. Because of the large atomic weight ($A = 208$) the deviations from a parabolic behavior are in most cases less than 1 keV. However for spectra taken at large scattering angles a systematic uncertainty should be kept in mind.

The parameters c_1, c_2 should be proportional to the magnetic field B except for slight variations in the order of $(E_x - E_x^{\mathrm{NDS}})/(E_p - E_x) = 10^{-4}$ because of the correction by the entrance quadrupole and hysteresis effects. By keeping the magnetic field unchanged and only varying the proton energy E_p, different regions of excitation energies can be compared (often jumping from one IAR to another). In this case variations of less than 10^{-5} may be achieved [34].

A final accuracy $\delta E_x < 1.0$ keV for well isolated peaks with sufficiently good statistics, up to $\delta E_x \leqslant 0.1$ keV for peaks with high statistics is achieved. The accuracy does not much depend on the excitation energy up to $E_x = 8.2$ MeV, the maximum energy where data were taken both for ^{208}Pb(p, p') and ^{207}Pb(d,p).

3. GASPAN *options*

For close doublets either their energetic distance or their relative intensities can be determined more precisely by help of GASPAN.

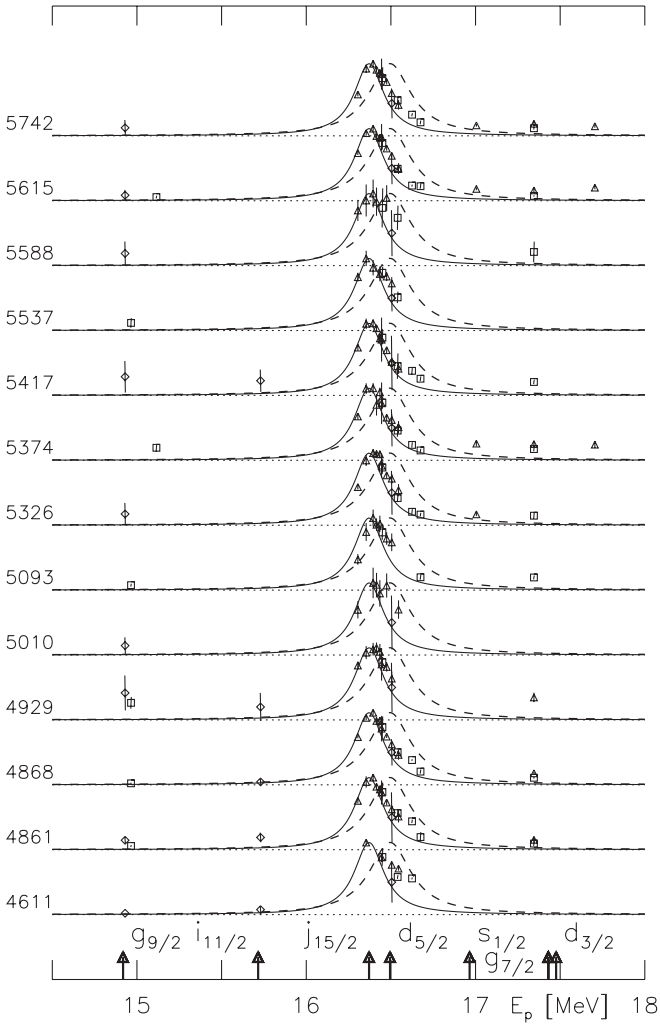

FIG. 10. For proton energies $14.5 < E_p < 18.0$ MeV, normalized excitation functions for states with energy label E given at left (Table IV). Lorentzian curves are calculated for the $j_{15/2}$ (drawn) and the $d_{5/2}$ (dashed) IAR [Eq. (8) with parameters from Table II]. All known IAR in ^{209}Bi are shown at bottom. Different regions of scattering angles are denoted by a triangle for $\Theta = 138^\circ$, a square for $\Theta = 88^\circ$, a diamond for $72^\circ < \Theta < 115^\circ$. They correspond to data from different beam times (see Sec. III F).

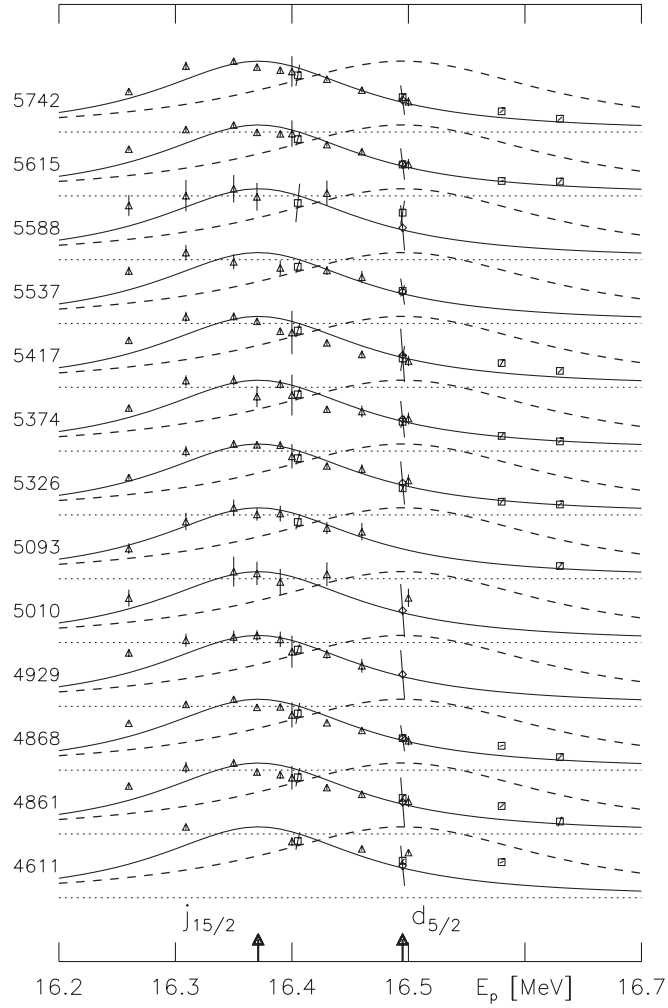

FIG. 11. Expanded view of Fig. 10 for proton energies $16.2 < E_p < 16.7$ MeV covering the $j_{15/2}$ and $d_{5/2}$ IAR. Positive and negative parity states are best discriminated by comparing the ratio of the cross sections at $E_p \approx 16.35, 16.60$ MeV.

The GASPAN option of fixed energy spacing [33] allows to determine the difference of one floating energy against a group of fixed excitation energies with a precision of about a tenth of the resolution. With sufficiently good statistics, spacings of less than 1 keV with an uncertainty of about 0.2 keV can be determined. By this method the excitation energies of the 5648, 5649 doublet are determined (Table III).

By using the same option, cross sections of a doublet with spacings 0.5–1.5 times the resolution may be determined with more reliability than with the option of floating energies for all levels.

C. Excitation functions

In four beam times of ^{208}Pb(p, p') experiments, different regions of scattering angles are covered. The excitation functions are fitted by a calculated Lorentzian with parameters from Table II [Eq. (8)] and normalized to the top of the $j_{15/2}$ IAR. For each beam-time a slightly different absolute proton energy is assumed, see Sec. III F. By taking the position of the $d_{5/2}$ IAR as reference all excitation functions are superimposed. Figures 10 and 11 show excitation functions for several states with selective excitation by the intruder IAR $j_{15/2}$.

The $j_{15/2}$ and $d_{5/2}$ IAR are separated by less than their width (Table II). Hence the cross section of negative parity states with significant fragments of the configurations $d_{5/2}\, lj$, $lj = p_{1/2}, f_{5/2}, p_{3/2}$, is still 50% of the maximum cross section near the top of the $j_{15/2}$ IAR. Vice versa for positive parity states, the cross section near the $d_{5/2}$ IAR is still about half of the maximum cross section on the $j_{15/2}$ IAR.

Because the total width $\Gamma^{\rm tot}_{d_{5/2}}$ of the $d_{5/2}$ IAR is much larger than $\Gamma^{\rm tot}_{j_{15/2}}$ for the $j_{15/2}$ IAR (Table II) the ratio of the cross section for a positive parity state excited by the $j_{15/2}$ IAR and a negative parity state excited by the $d_{5/2}$ IAR becomes the least at proton energies $E_p \approx 16.6$ MeV. In contrast, the ratio is larger at proton energies $E_p \approx 16.3$ MeV and thus less meaningful.

All positive parity states under discussion except for four doublets ($E_x = 4.928, 5.194, 5.214, 5.648$ MeV, see Sec. III D) are resolved by the Q3D experiments, see however the discussion of an atomic effect in Appendix B.

Although the mean cross sections are small, $\sigma^{\text{avg}} < 30\,\mu$b/sr [Eq. (11)], the off resonance cross section at low proton energies $E_p \ll (E^{\text{res}} - \Gamma^{\text{tot}})$ is determined to be mostly less than 20% of the maximum. At higher proton energies $E_p \gg (E^{\text{res}} - \Gamma^{\text{tot}})$ it is still about 30% except for the lowest 8^+ state which has a considerable direct-pp' component [4] or where the experimental uncertainties are large. The asymmetry of the excitation function is explained by the penetrability increasing with the bombarding energy E_p [5].

D. Doublets

The nomen doublet denotes two or more states not resolved by some experiment. The nomen multiplet is reserved for some SSM configuration $LJ\,lj$ with spins $I = |J - j|, \ldots, J + j$.

Disentangling the cross sections of doublets is difficult if either the distance is small or the excitation of the individual states differs considerably. For example, in Fig. 7 the ratio of the cross section for the 5010 9^+ state to that for the 4974 3^- state is about 1 : 100. In Fig. 8 the distance between the 5648 and 5649 states is less than 0.5 keV.

Positive parity states excited by the $j_{15/2}$ IAR have cross sections which are at average a factor 10–300 smaller than negative parity states excited by all other IAR. Especially, the $d_{5/2}$ IAR has a distance of less than half the resonance width Γ^{tot} from the $j_{15/2}$ IAR. Therefore the cross sections of states weakly excited by the $d_{5/2}$ IAR often compete with those from positive parity states excited by the $j_{15/2}$ IAR.

Some doublets are not resolved in the Q3D magnetic spectrograph. However, the selective excitation by different IAR leads to a shift of the excitation energy in dependence of both the bombarding energy E_p and the scattering angle Θ. Figure 8 shows spectra of a quintuplet of states, $E = 5640, 5642, 5643, 5648, 5649$ [6]. The 5648, 5649 states discussed below (Sec. III D) are resolved by the systematic shift of the excitation energy with the proton energy near the $j_{15/2}$ IAR (Table III).

In case the distance between two members of a doublet with about equal cross sections is more than half the resolution (i.e., $\delta E_x \gtrsim 2$ keV), a GASPAN option allows to determine the cross section of each member (Sec. III B3). In case the excitation functions of the two members of the doublet differ, by deconvoluting with the shape of the excitation functions measured for (ensembles of) other states, the angular distributions for the two members can be disentangled. If one member may be assumed to be excited by direct-pp' essentially only, the angular distribution of the direct-pp$'$ member may by determined far off the IAR. The angular distribution of the other member can then be determined by deconvoluting with the measured shape of the excitation function, too.

The $4.842 + 4.861 + 4.868, 4.974 + 4.995, 5.517 + 5.537$, $5.564 + 5.588, 5.886 + 5.899, 5.924 + 5.928$ MeV doublets. Some positive parity state are within less than about 20 keV above states strongly excited by the $d_{5/2}$ IAR (Figs. 4–9). By fitting the satellite peaks from L electrons for the strong peaks in the same region in a similar manner (Appendix B), the cross sections of the 4861, 4868, 4995, 5537, 5588, 5899, 5928 states are obtained. In some cases weak peaks from other states between the doublet states [6] have to be included, too.

The 5924 state is strongly excited by the $d_{5/2}$, $d_{3/2}$ IAR. The excitation energy and the mean cross section of the 5928 state can be determined only with a large uncertainty (Table III, Fig. 9).

The $4.928 + 4.929$ MeV doublet. NDS2007 assigns spin 2^+ to the 4928 state. The level at $E_x = 4.928$ MeV is resonantly excited by the $j_{15/2}$ IAR (Fig. 11). For some ranges of scattering angles the off-resonance cross section is larger than expected by assuming a Lorentzian shape of the excitation function. The variation of the excitation energies with the proton energy E_p or the scattering angle Θ is less than 0.5 keV. In sect. IV G arguments are given for a doublet of two states with spins 2^+ and 5^+.

The $5.193 + 5.194 + 5.195$ MeV doublet. The 5193, 5194, 5195 states are recognized by NDS2007 as a triplet with spins 5^+, $\{3^-, 4^-\}$, 7^+, respectively (Table III). The 5193, 5194, 5195 states are not fully resolved by IAR-pp'. The excitation energies change with the proton energy E_p or the scattering angle Θ by about 0.4 keV in an uncorrelated manner. The 5193 state is weakly excited by IAR-pp'.

One state of the $5194 + 5195$ doublet has negative parity since it is excited by the $d_{5/2}$ and the $g_{7/2}$ IAR, the other state has positive parity since it is excited by ^{209}Bi(d,^{3}He) and ^{209}Bi(t, $\alpha\,\gamma$). On top of the $j_{15/2}$ IAR, the cross section of the doublet is enhanced by about 20% relative to other proton energies.

The $5.213 + 5.214 + 5.216$ MeV doublet. The 5213, 5214, 5216 states are recognized by NDS2007 as a doublet with spins 6^+, (5^-), 4^+, respectively (Table III). By IAR-pp' the 5213, 5214 states are not resolved. The close-lying 5216 4^+ state is excited with a mean cross section below 0.5 μb/sr.

The variation of the excitation energies with the proton energy E_p or the scattering angle Θ is less than 0.5 keV. The 5213 state has positive parity since is it excited by the $j_{15/2}$ IAR. The 5214 state has negative parity since it is excited by the $g_{9/2}$, $d_{5/2}$ and $g_{7/2}$ IAR.

The $5.648 + 5.649$ MeV doublet. The 5648, 5649 states are not resolved by IAR-pp' (Fig. 8). On top of the $j_{15/2}$ IAR, however, the mean excitation energy is higher by 0.5 keV than on top of all other IAR. The 5648 state is excited both by the $g_{9/2}$ and $d_{5/2}$ IAR, the 5649 state by the $j_{15/2}$ IAR. For both states, in the region $16.1 \lesssim E_p \lesssim 16.6$ MeV the mean cross section σ^{mean} [Eq. (10)] is similar.

A further difficulty arises from the neighborhood to the $5642 + 5643$ doublet. On top of the $d_{5/2}$ IAR at some scattering angles, the 5643 state is often stronger excited than the $5648 + 5649$ doublet (Fig. 8).

The centroid energies of the 5642, 5643 states and the 5648, 5649 states are determined as function of the proton energy E_p and the scattering angle Θ. Systematic variations are found. By comparison to NDS2007 the excitation energies of the 5642 and 5648 states are verified within the experimental uncertainties (Table III).

The energy of the 5643 state is determined with higher precision than by NDS2007, the 5649 state is newly identified. For the 5643 state being excited by the $d_{5/2}$ IAR spins 6^-, 7^- are excluded.

The 5.989 + 5.993 MeV doublet. The 5989, 5993 states are not resolved by ^{208}Pb(e,e') [6,35]. They are recognized as two states with different parity. Namely, the 5989 state is excited by the $j_{15/2}$ IAR and hence has positive parity while the 5993 state is excited by the $g_{9/2}$, $d_{5/2}$ IAR and the $g_{7/2} + d_{3/2}$ doublet IAR and hence has negative parity (Table III).

E. Cross sections

As an intruder, the $j_{15/2}$ IAR may excite positive parity states solely. On top of the $j_{15/2}$ IAR only states containing admixtures of particle-hole configurations built with a $p_{1/2}$, $f_{5/2}$, $p_{3/2}$ hole may produce measurable cross sections. Therefore states with spins from 5^+ to 10^+ may be detected. Mostly, we do not discuss positive parity states with other spins.

We note that the cross section for neutron particle-hole states with configurations $LJ\, i_{13/2}$ built with the *intruder hole* are calculated [7] to be less than 1 μb/sr even for the $g_{9/2}$ and $d_{5/2}$ IAR created strongly.

Most of the cross sections for states with configurations $j_{15/2}\, lj$, $lj = p_{1/2}$, $f_{5/2}$, $p_{3/2}$, built with the *intruder particle* are of the order of 1–20 μb/sr while in the Q3D experiments a background of at least 0.1 μb/sr is seen. Since in addition several different targets were used, the angular distributions are mostly measurable with a precision of larger than 10% even in case of good statistics.

Often, the angular distributions have extreme shapes with a steep increase or decrease at scattering angles near $\Theta = 0^\circ$ and $\Theta = 180^\circ$. The Q3D experiments do not allow measurements beyond $\Theta = 140^\circ$. Measurements in the range $\Theta = 0^\circ$–35° become difficult because of the increasing background from stray scattering of protons and the increasing background from contamination lines due to light nuclei in the target (^{1}H, ^{2}H, ^{12}C, ^{14}N, ^{16}O, ^{40}Ar). Therefore the comparison of angle integrated cross section $\sigma^{\rm avg}$ [Eq. (11)] instead of mean cross sections $\sigma^{\rm mean}$ [Eq. (10)] may have large systematic errors.

F. Resonance energy

Among the positive parity states, early experiments (with a resolution of 27–35 keV) resolved only the 4611 8^+_1 state [4]. Since it is well isolated, from the excitation function taken for $15.8 < E_p < 16.6$ MeV at scattering angles $\Theta = 90^\circ, 158^\circ$, the IAR parameters for the $j_{15/2}$ IAR were determined. The 4611 state is excited by direct-pp', too, distorting the resonance curve.

The absolute value of the resonance energy depends on the method describing the asymmetry of the excitation function [4,5]. Variations of the parameters within the uncertainties change the position of the resonance by up to 30 keV.

Because of different focusing procedures, the absolute value of the proton energy changes by up to 20 keV while comparing results from different beam times. In Figs. 10 and 11, a global shift of the proton energy has been applied for each beam time.

The comparison of data taken with different accelerators [Seattle [4] and München (this work)] reveal a systematic difference of the absolute proton energies by about 10 keV. Therefore the resonance energy of the $d_{5/2}$ IAR determined by [4] is taken as reference (Table II).

The parameters determined for a large ensemble of states from this work (Tables III and IV) are

$$\begin{aligned} E^{\rm res}{}_{j_{15/2}} &= 16.375 \pm 0.010\,{\rm MeV}, \\ \Gamma^{\rm tot}_{j_{15/2}} &= 210 \pm 10\,{\rm keV}. \end{aligned} \tag{18}$$

The resonance energy $E^{\rm res}_{j_{15/2}}$ is 40 keV higher than obtained by the early study of the lowest 8^+ state [4]. For this reason the first Q3D data [5] missed the top of the $j_{15/2}$ IAR. The IAR parameters [Eq. (18)] agree with [4] but are more precise.

IV. RESULTS

The final goal of this work is the determination of the structure of all positive parity particle-hole states in ^{208}Pb below $E_x < 6.1$ MeV. However in order to shorten the discussion, only the states with spins 5^+–10^+ and their major configurations are investigated.

As shown for ^{140}Ce, spin and structure of particle-hole states can be derived [8] from the coefficients A_K, $K = 0, 2, \ldots$, of a fit of angular distributions of (p,p') on some IAR [Eq. (9)]. For the particle-hole states in ^{208}Pb the method was applied, too, and yields the structure of the 20 lowest negative parity states [16,17] and the multiplets [Eqs. (4), (5)] built with the $i_{11/2}$ particle [5].

Because this work comprises data from separate beam times with several different targets, the determination of angular distributions is difficult. In addition the cross sections of interest are below 30 μb/sr. Here we use the angle integrated cross section $\sigma^{\rm avg}$ [Eq. (11)]. Only for the determination of the spin for the 5615 state, the shape of the angular distributions taken on different IAR is considered [5].

A future analysis of the angular distributions will yield the structure of almost all positive parity states in ^{208}Pb with spins 5^+–10^+ below $E_x < 6.1$ MeV, a few more than presented here.

A. Reaction mechanism

Excitation functions are measured for proton energies $14.8 < E_p < 18.1$ MeV (Figs. 10 and 11). For almost all positive parity states with spins 5^+–10^+, the ratio of the off-resonance cross section to the maximum cross section on top of the $j_{15/2}$ IAR is about 0.2 : 1 if the statistics are sufficient (Table IV).

From the comparison of data taken at backward angle $\Theta = 138^\circ$ to data taken at $\Theta \approx 40^\circ$, for all states an asymmetry of the angular distribution can be excluded for angles $\Theta \gtrsim 30^\circ$ except for the 4424 6^+_1 state and the 4611 8^+_1 state. Therefore except for these two states, we assume the angular distribution of all states with spin 5^+–10^+ to be described as a purely resonant reaction [5,8] without a direct-pp' component.

B. Identification of positive parity states

Below $E_x < 6.1$ MeV, from the SSM (Table I) 36 positive parity states with spins 5^+–10^+ are expected to be described by an unitary transformation of up to eight configurations for each spin. In addition 2p-2h states with spins 5^+–10^+ are expected [22,24] none of which is firmly identified up to now.

Positive parity states are identified by their selective excitation on top of the $j_{15/2}$ IAR. Figures 10 and 11 show some excitation functions.

Spectra near the $j_{15/2}$ IAR were taken for excitation energies $4.5 < E_x < 6.1$ MeV. In this region about 130 levels are identified. (For $4.4 < E_x < 6.1$ MeV the SSM predicts 50 states with positive parity and spins 1^+–12^+, 50 states with negative parity and spins 0^-–8^-.)

Excitation functions for each level were studied for several scattering angles. In each beam time different ranges of scattering angles were used, especially one beam time was performed at $\Theta = 138°$, the technically most extreme backward angle.

More states are identified to have positive parity than shown in Table IV. However in several cases the identification is not convincing, either because the statistics are too low or because of difficulties in resolving doublets. Especially excitation energy regions in a distance of about 10–20 keV above states with large components $LJp_{1/2}$, $LJp_{3/2}$, $LJ = g_{9/2}, d_{5/2}, s_{1/2}$, $g_{7/2}$, $d_{3/2}$ are difficult to study because of the presence of satellites from the knockout of L electrons (Appendix B). In Figs. 6, 7, and 9 such satellites next to the 4841, 4868, 4974, 5038, 5886, 5924, 5969 states are considered.

The cross sections of positive parity states built with the regular particles ($LJ \neq j_{15/2}$) and the intruder hole $i_{13/2}$ are calculated to be less than 1 μb/sr [7]. Only by the direct-pp' reaction some positive parity states with dominant $g_{9/2}i_{13/2}$ structure are observed, namely the lowest states with natural parity, the 4086 2^+, 4324 4^+, 4424 6^+ states [6].

Below $E_x < 6.1$ MeV, NDS2007 lists about 40 states with either firm positive parity assignment or possible positive parity. Among them there are about 20 states with spins 5^+–10^+. In addition some states attributed negative parity may have positive parity. Tables III and IV show the states identified to have positive parity together with states belonging to doublets with positive parity states.

C. Verification of identifications by NDS2007

In NDS2007 positive parity states are identified mainly by data from ^{209}Bi(d,^{3}He) [30], ^{209}Bi(t, $\alpha\gamma$) [31], and ^{208}Pb(e,e') experiments [35].

The 5615 7^+ state is already discussed in [13,14]. In [5] the 4929, 4995, 5010, 5069, 5093, 5195 are already recognized to resonate on top of the $j_{15/2}$ IAR. In NDS2007, correspondence from the preliminary evaluation of data to the 4611, 4861, 4868, 5326, 5339, 5374, 5417, 5537, 5615, 5649, 5742, 5764 states [5] is given as a private communication.

In the following, we accept the spin assignment to the 4424, 4611, 4861, 4868, 4895, 5010, 5069, 5093, 5162, 5193, 5195, 5213, 5339, 5537, 5928 states [6].

The 4424 6^+ and 4611 8^+ states. The 4424 6^+_1 state has a strong direct-pp' component. Similar to the 4086 2^+_1, 4324 4^+_1 states, the angular distribution is dominated by an asymmetric shape (with a steep raise toward forward angles) with a nonresonant dependence on the proton energy E_p. The 4611 8^+_1 state has a direct-pp' component, too, the resonance behavior dominates, however [4].

The 10^+ states and states with major $h_{9/2}h_{11/2}$ fragments. The structure of the 4895, 5069, 5537, 5928 states with spin 10^+ is derived by [36]. The 5537 10^+_3 state is verified to contain the major fraction of the $j_{15/2}f_{5/2}$ strength; the 4985 10^+_1, 5069 10^+_2 states contain minor fractions (Tables III and IV). The 5928 10^+_4 state is barely seen in a few spectra of ^{208}Pb(p,p').

The spin assignments to the states 5162, 5093, 5193, 5195, 5213, 5339 with dominant configuration $h_{9/2}h_{11/2}$ and spins $9^+, 8^+, 5^+, 6^+, 7^+, 8^+$, respectively, is accepted. The low mean IAR-pp' cross section is compatible with the assignments (Table III). The 5193 5^+ state near the 5194 + 5195 doublet is weakly excited by the $j_{15/2}$ IAR. For the 5193 + 5194 + 5195 and 5213 + 5214 + 5216 doublets a complication arises since in between there is a negative parity state, see Sec. III D.

D. Identifying states with major $j_{15/2}p_{1/2}$ strength

NDS2007 shows the 4611, 4861, 4868 states to have spins 8^+, 8^+, 7^+, respectively. The ratio of the mean cross sections σ^{avg} from ^{208}Pb(p,p') [Eq. (11)] compares well to the ratio of the mean cross sections $\sigma^{\text{avg}}_{(d,p)}$ from ^{207}Pb(d,p) [Eq. (13)]. Hence the admixture of configurations $j_{15/2}f_{5/2}$ and $j_{15/2}p_{3/2}$ to the 4611, 4861, 4868 states is small. This is especially true for $j_{15/2}p_{3/2}$ because of the large single particle width $\Gamma^{\text{s.p.}}_{p_{3/2}}$ (Table II).

By comparison to the SSM (Table I), the two lowest 8^+ states essentially share the two configurations $g_{9/2}i_{13/2}$ and $j_{15/2}p_{1/2}$ while the lowest 7^+ state may be assumed to contain little admixtures of other configurations.

E. Identifying states with major $j_{15/2}p_{3/2}$ strength

The 5615, 5649, 5742, 5764 states stick out by their large mean cross sections (Table III). By using the ratio of the s.p. widths $\Gamma^{\text{s.p.}}_{p_{3/2}}/\Gamma^{\text{s.p.}}_{p_{1/2}}$ (Table II), in comparison to the 4611, 4861, 4868 states containing most of the $j_{15/2}p_{1/2}$ strength, a prominent admixture of $j_{15/2}p_{3/2}$ is assigned to the 5615, 5649, 5742, 5764 states.

From the ^{209}Bi(d,^{3}He) data [30,32], for the 5615, 5764, 5742 states an admixture of $h_{9/2}h_{11/2}$ is determined to be less than 1% (Table III). The proton transfer data for the unresolved 5648 + 5649 doublet yield no decisive information about the 5649 state (Sec. III D).

From the ^{207}Pb(d,p) data, for the 5615, 5649, 5764 states an admixture of $j_{15/2}p_{1/2}$ is determined to be less than 2% (Table IV) while the 5742 state is excited by ^{207}Pb(d,p) with a strength of about 5%. By the steep increase of the cross section for $\Theta = 20°$–$30°$, the orbital angular momentum for the 5742 state is determined as $l = 7$, hence the spin is either 7^+ or 8^+.

(i) The 5764 state is assigned spin 6^+ by NDS2007. The mean cross section corresponds to about half of the $j_{15/2}p_{3/2}$ strength.

(ii) For the 5742 state, the angular momentum $L = 9$ from ^{208}Pb(p,p') at $E_p = 35$ MeV [25] favors the

assignment of spin 8^+ and hence spin 7^+ is excluded. The mean cross section of the 5742 state corresponds to about half of the $j_{15/2}p_{3/2}$ strength.

(iii) The sum of the $j_{15/2}p_{3/2}$ strength in the 5615, 5742 states is calculated to exceed unity for any spin; hence the two states have different spins.
The shape of the angular distribution for the 5615 state excludes spin 6^+, 9^+ by comparison to calculations for the pure configuration $j_{15/2}p_{3/2}$. The anisotropy coefficients for spin 6^+, 7^+, 8^+, 9^+ are $A_2/A_0 = +0.600$, -0.388, -0.576, $+0.412$, respectively; therefore for states with spins $I = 7, 8$ the angular distributions have a *maximum* at 90° while for states with spins $I = 6, 9$ the angular distributions have a *minimum* at 90° and are raising strongly toward forward angles [5].
From the angular distribution for the 5615 state a value $A_2/A_0 = -0.5 \pm 0.3$ is derived [Eq. (9)]. Hence the 5615 state is assigned spin 7^+ and shown to nearly exhaust the $j_{15/2}p_{3/2}$ strength.
(For the 5764 6^+ state a value $A_2/A_0 = +0.3 \pm 0.2$, for the 5742 8^+ state a value $A_2/A_0 = -0.6 \pm 0.2$ is derived, confirming the spin assignments.)

(iv) The 5989 and 5993 states have negative and positive parity, respectively (Sec. III D).
The 5993 state is assigned 2^- to 5^- because of the excitation by the $d_{5/2}$ IAR and the $g_{7/2}$, $d_{3/2}$ doublet IAR. The branching of the γ intensity in ^{207}Pb($d,p\,\gamma$) can be explained, especially if the 5194 + 5195 doublet is assumed to contain a 3^- or 4^- state (Table III).
The level at 5.993 MeV, to which spin 6^+ is assigned by the ^{208}Pb(e,e') experiment [6] and to which an angular momentum $L = 6$ is determined by the ^{208}Pb(p,p') experiment at $E_p = 35$ MeV [25] is identified with the 5989 state.

(v) The large cross section of the 5649, 5899 states excludes spins 6^+, 7^+. Spin 8^+ is ruled out for either of the two states. In a tentative manner spin 9^+ is assigned to both the 5649 and the 5899 state.

(vi) The order number N (Table IV) for the 5615, 5649, 5742, 5764, 5899, 5989 states with spins 7^+, $(9)^+$, 8^+, 6^+, $(9)^+$, 6^+, respectively, is assigned by comparison to Table I.

F. Identifying states with major $j_{15/2}f_{5/2}$ strength

All four 10^+ states are known (Sec. IV C). Therefore in the region of $E_x \approx 5.3$ MeV states excited by the $j_{15/2}$ IAR are expected to contain large fractions of the configuration $j_{15/2}f_{5/2}$ with spins 5^+ to 9^+.

The 5417 6^+ and the 5339 8^+ states [6] are excited by the $j_{15/2}$ IAR with a cross section corresponding to about half the $j_{15/2}f_{5/2}$ strength. Whereas the 5339 8^+ has a considerable $h_{9/2}h_{11/2}$ component, the 5417 6^+ state is weakly excited by ^{209}Bi(d,^{3}He) (Table III).

Either cross section of the 5326, 5374 states exceeds the strength of half the $j_{15/2}f_{5/2}$ strength for spin 6^+ or 8^+. Each one exceeds the cross section of a pure 5^+ state, too. Hence the 5326, 5374 states are assigned spin 7^+ or 9^+ (Table III). The mean cross section indicates each of the two states to nearly exhaust the $j_{15/2}f_{5/2}$ strength of either spin. From ^{209}Bi(d,^{3}He) a weak $h_{9/2}h_{11/2}$ admixture is derived.

Only the 5374 is excited by ^{207}Pb(d,p), the orbital angular momentum is determined to be $l = 7$, hence the spin is 7^+. Correspondingly the 5326 state is assigned spin 9^+.

The order number N (Table IV) for the 5326, 5339, 5374, 5417 states with spins 9^+, 8^+, 7^+, 6^+, respectively, is assigned by comparison to Table I.

The 5588 state is excited by the $j_{15/2}$ IAR with a considerable mean cross section (Table III). The excitation by ^{207}Pb(d,p) is very weak and no excitation by ^{209}Bi(d,^{3}He) is seen (Table III). Spin 5^+ is tentatively assigned since no other state in the region $4.9 \lesssim E_x \lesssim 5.6$ is left as a candidate for a $j_{15/2}f_{5/2}$ state with spin 5^+. The assignment yields a rather pure $j_{15/2}f_{5/2}$ configuration.

G. Identifying states with major $g_{9/2}i_{13/2}$ strength

The 4086 2_1^+, 4324 4_1^+, 4424 6_1^+ states are excited near the $g_{9/2}$ IAR primarily by the direct-pp' reaction; the resonant cross section is calculated to be negligible (Sec. III E). Weak admixtures of $h_{9/2}h_{11/2}$ are determined [30,31]. The 4086, 4324, 4424 states are assumed to mainly consist of the lowest positive parity particle-hole configuration $g_{9/2}i_{13/2}$ (Table I).

The 4611 8_1^+ state has a strong $j_{15/2}p_{1/2}$ component (Sec. IV D). The 4895 10_1^+ state has a weak $j_{15/2}f_{5/2}$ component (Table III). Both states are assumed to contain a large $g_{9/2}i_{13/2}$ strength.

Among the unnatural parity states with dominant configuration $g_{9/2}i_{13/2}$ only the 5010 9^+ state is known [6]. Figure 7 shows its fully resolved peak. Figures 10 and 11 show a resonance although the mean cross section on top of the $j_{15/2}$ IAR is only 1.5 μb/sr (Table IV). Less than 20% of the $j_{15/2}f_{5/2}$ or 5% of the $j_{15/2}p_{3/2}$ strength is contained in the 5010 9^+ state. From ^{209}Bi(d,^{3}He) a weak $h_{9/2}h_{11/2}$ admixture is derived (Table III).

The 4995 state is excited by the $j_{15/2}$ IAR with a cross section of about 2 μb/sr (Table III). From ^{209}Bi(d,^{3}He) a weak $h_{9/2}h_{11/2}$ admixture is derived. From ^{208}Pb(p,p') at $E_p = 35$ MeV [25] the angular momentum is determined as $L \geqslant 7$. Because the states with major configuration $g_{9/2}i_{13/2}$ and spins 6^+, 8^+, 9^+, 10^+ are known, spin 7^+ is assigned. Less than half the $j_{15/2}f_{5/2}$ strength is contained in the 4995 7^+ state. An admixture of $j_{15/2}p_{1/2}$ is weak (Tables III and IV). An admixture of $j_{15/2}p_{3/2}$ is less than 10%. By SSM (Table I) a dominant configuration $g_{9/2}i_{13/2}$ is assigned.

The 4928 state is known to have spin 2^+ [6]. Indeed it is excited at all proton energies (Fig. 10). The angular distribution shows the forward peaking typical for a direct-pp' reaction. However, a resonance effect on top of the $j_{15/2}$ IAR is detected (Fig. 11, Table IV). Hence a 4928 + 4929 doublet is assumed (Sec. III D).

On top of the $j_{15/2}$ IAR about half of the mean cross section of the 4929 state (about 1.5 μb/sr) can be contributed to a $j_{15/2}\,lj$ component. Because most of the $j_{15/2}f_{5/2}$ strength is already located in other states with spins 5^+–10^+ (Table IV), spin 5^+ and a dominant configuration $g_{9/2}i_{13/2}$ is assigned

to the 4929 state by comparison to the SSM (Table I). The $j_{15/2}f_{5/2}$ strength in the 4929 5^+ state is less than 30%.

The order number N (Table IV) for the 4424, 4611, 4895, 4929, 4995, 5010 states with spins 6^+, 8^+, 10^+, $(5)^+$, $(7)^+$, 9^+ respectively, is assigned by comparison to Table I.

H. Other positive parity states

Among the high spin positive parity states, from ^{208}Pb(e,e') [6,35], three 9^+ states at $E_x = 5010$, 5260, 5954 keV (Table III) and two 11^+ states at $E_x = 5291$, 5860 keV are reported. (In Figs. 8 and 11 of [35] two different data sets for the 5291 state are displayed. From the systematics of the calculations one may conclude that Fig. 8 displays the reported 5260 9^+ state while Fig. 11 displays the reported 5291 11^+ state.)

The current evaluation of IAR-pp' does not indicate the detection of any 11^+ state. The 5010 9^+ state with main configuration $g_{9/2}i_{13/2}$ is confirmed, see Sec. IV G.

The identification of a 5260 state to have spin 9^+ and to consist of the $h_{9/2}h_{11/2}$ configuration conflicts with the identification given for the 5162 state (Sec. III D), even within the resolution of about 50 keV.

The identification of the 5954 state assigned 9^+ with $i_{11/2}i_{13/2}$, $f_{7/2}h_{11/2}$ configurations may correspond to the 5958 state (Table III, Fig. 9), but the few ^{208}Pb(p,p') data are not conclusive.

In the region $6.00 < E_x < 6.15$ MeV three states with possible positive parity are reported by NDS2007, $E_x = 6037.5$ keV $(5^+, 6^+)$, $E_x = 6068.5$ keV $(5^+, 6^+)$, $E_x = 6101.1$ keV (5^+). All three levels are observed in IAR-pp' with mean cross sections of about 2 μb/sr in a region which is extremely difficult to analyze. Namely on the $d_{5/2}$ IAR the 6012 state has the largest mean cross section of all states at $2.4 < E_x < 8.2$ MeV (about 350 μb/sr) and hence several satellites from L electrons have to be considered (Appendix B). In addition the 6087 state is excited by the $d_{5/2}$ IAR strongly, too. Because of their close neighborhood, the selective excitation of the 6037, 6068, 6101 states by either the $j_{15/2}$ or the $d_{5/2}$ IAR cannot be decided at the current stage of evaluation (Fig. 5).

V. CONCLUSION

For several proton energies $14.8 < E_p < 18.1$ MeV and at some scattering angles 20°–138°, excitation functions and angular distributions of ^{208}Pb(p,p') via IAR in ^{209}Bi were measured. In the doubly magic nucleus ^{208}Pb below $E_x <$ 6.1 MeV, 27 states with spins 5^+–10^+ are identified.

By using the Q3D magnetic spectrograph of the Maier-Leibnitz-Laboratorium at München, the excitation energy is determined with a precision of 0.1 keV for strongly excited states in ^{208}Pb. Several doublets with spacings less than 0.5 keV are resolved by their excitation in IAR with different parity or by exhibiting a resonance effect in different IAR.

States with parts of the $j_{15/2}p_{1/2}$, $j_{15/2}f_{5/2}$, $j_{15/2}p_{3/2}$ strengths are identified by the selective excitation in the $j_{15/2}$ intruder IAR. Besides several states with dominant configurations $j_{15/2}\,lj$, the examination of minor such admixtures allows to identify states with major *proton* particle-hole configurations or states consisting mainly of the particle-hole configurations $LJ\ i_{13/2}$ built with the *neutron intruder hole* $i_{13/2}$.

From the experimental data of this work and by comparison to NDS2007 data, 27 positive parity states in ^{208}Pb have been identified and their dominant configuration determined. Among the 36 positive parity states in ^{208}Pb with excitation energies $E_x < 6.1$ MeV and spins 5^+–10^+ predicted by the SSM, only nine states are not yet identified. Assignments for 18 positive parity states given in NDS2007 are confirmed. In addition nine positive parity states are newly identified.

ACKNOWLEDGMENTS

We thank T. von Egidy, P. Grabmayr, and G. Mairle for discussions. We thank the accelerator operators for providing finely tuned stable beams. We are grateful to the target makers for providing clean ^{208}Pb targets. This work has been supported by DFG Br799/20-1 and DFG Gr 894/3 and US DOE Grant No. DE-FG02-91ER-40609.

APPENDIX A: THE GASPAN FIT FUNCTION

The peak shape function $y(j)$ is defined for a region of n consecutive channels j starting at channel j_0 with N peaks. The fit of the measured data points $x(j)$ utilized in GASPAN is

$$y(j) = \sum_{i=1}^{N} A_G(i)\left\{ e^{-z(i,j)^2/\delta(i)^2} + A_T\, e^{z(i,j)/\nu}\,\mathrm{erfc}\left[\frac{z(i,j)}{\delta(i)} + \frac{\delta(i)}{2\nu}\right]\right\} + \sum_{l=0}^{l_{\max}} A_B(l)\,(j - \langle j\rangle)^l, \tag{A1}$$

$$z(i,j) = j - A_p(i), \quad \langle j\rangle = \frac{1}{n}\sum_{i=1}^{n}(i + j_0 - 1). \tag{A2}$$

The parameters A_G, A_P, δ define the strength, position, and width of the Gaussian peak, A_T, ν the strength and decay constant of the tail, A_B the background. Here erfc is the complementary Gaussian error function

$$\mathrm{erfc}(a) = \frac{2}{\sqrt{\pi}}\int_a^\infty e^{-t^2}dt. \tag{A3}$$

In an iterative manner, the parameters A_G, A_P, A_T, A_B, δ, ν are obtained by minimizing the fit criteria

$$\chi^2/f = \sum_{j=j_0}^{j_0+n-1}\Delta^2(j), \tag{A4}$$

$$\Delta(j) = \frac{y(j) - x(j)}{\sigma(j)}, \tag{A5}$$

where $\sigma^2(j)$ is the variance of the data $x(j)$. The fit criterion Eq. (A4) should become close to $\chi^2/f = 1$, the deviation of the residuum spectrum $\Delta(j)$ should be below two standard errors $\sigma(j)$ everywhere,

$$-2 \lesssim \Delta(j) \lesssim +2 \tag{A6}$$

and not vary in a systematic manner anywhere. Except for the smooth background defined by a polynom with degree $l_{\max}$, all parameters are subject to constraints: $A_G(i) > 0$, $j_0 < A_P(i) < n$ or fixed, $A_T > 0$ or fixed, $\delta(i) > 0$ or fixed, $\nu > 0$ or fixed.

APPENDIX B: ATOMIC ELECTRONS AND ^{208}Pb(p,p')

In the analysis of the Q3D data, a careful inspection of the dependence of the excitation energy on both the proton energy E_p and the scattering angle has to take into account a specific experimental difficulty which finally limits the resolution of the Q3D magnetic spectrograph [13,37].

In the inelastic proton scattering on ^{208}Pb, the 82 electrons in the lead atom are affected, too,

$$^{208}_{82}\mathrm{Pb}(p, p' + ze^-)^{208}_{82}\mathrm{Pb}^{z+}, \quad z = 0, 1, 2, \ldots . \qquad \text{(B1)}$$

Satellites to each peak are produced since electrons from various atomic subshells are expelled. The intensity of each satellite peak depends on the mean number $\langle z \rangle$ of separated electrons and their binding energies, the proton energy $E_{p'}$ and the scattering angle Θ, but not on the target thickness.

The binding energy of the L_I, L_{II}, L_{III} electrons is 13.06, 15.20, 15.86 keV, respectively. The M electrons with 3 keV binding energy and the outer even less bound electrons are not resolved. The K electrons with 88 keV binding energy are never observed, since the intensity of such a peak is much less than for the other electrons and since in such a large distance from the main peak rarely no peak from ^{208}Pb(p, p') is present. Note that the mean distance of nuclear states in ^{208}Pb for $3.9 < E_x < 6.1$ MeV is about 10 keV becoming even less for higher excitation energies [6].

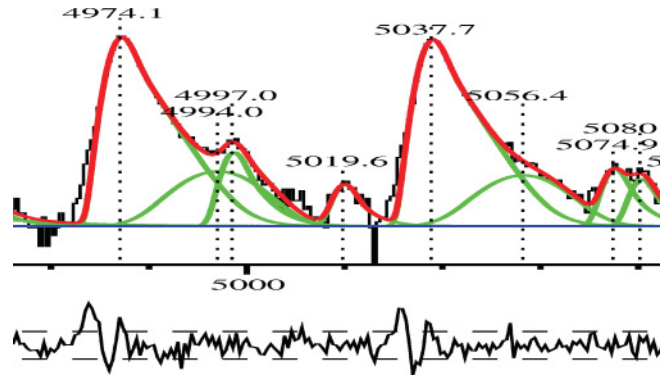

FIG. 12. (Color online) Excerpt of a ^{207}Pb(d,p) spectrum taken at $\Theta = 30^\circ$ and $E_d = 22$ MeV. The exponential tail [Eq. (A3), linear in this logarithmic plot] is followed along almost the full peak-to-valley ratio of 2000. The 4997, 5020 levels belong to ^{206}Pb(d,p); the 4974, 5038, 5075, 5080 levels belong to ^{207}Pb(d,p). The broader 4994, 5056 levels are the result of the pragmatic fit of the L_I, L_{II}, L_{III} lines from the electron knockout (Appendix B). At bottom the residual spectrum $\Delta(j)$ is shown [Eq. (A5)]; the dashed lines show the values $\Delta(j) = \pm 2\sigma$. The systematic variation of the residuum spectrum at the low energy side may be improved by including another tail A_T [Eqs. (A1), (A3)].

Therefore the first satellite peak is found in a distance of about 15 keV to the main peak with an intensity in the order of a few percent, the next peaks in about 30, 45 keV distances with less intensity [13]. A pragmatic procedure has been developed to fit the spectra by GASPAN [33] by adding a secondary peak in a mean distance of about 15 keV with about 3–4 times the width of the main peak if the statistics are sufficiently high, see Fig. 12.

[1] C. F. Moore, J. G. Kulleck, P. von Brentano, and F. Rickey, Phys. Rev. **164**, 1559 (1967).
[2] P. Richard, W. G. Weitkamp, W. Wharton, H. Wieman, and P. von Brentano, Phys. Lett. B **26**, 8 (1967).
[3] S. A. A. Zaidi, L. J. Parish, J. G. Kulleck, C. F. Moore, and P. von Brentano, Phys. Rev. **165**, 1312 (1968).
[4] W. R. Wharton, P. von Brentano, W. K. Dawson, and P. Richard, Phys. Rev. **176**, 1424 (1968).
[5] A. Heusler, G. Graw, R. Hertenberger, F. Riess, H.-F. Wirth, T. Faestermann, R. Krücken, J. Jolie, D. Mücher, N. Pietralla, and P. von Brentano, Phys. Rev. C **74**, 034303 (2006).
[6] M. J. Martin, Nucl. Data Sheets **108**, 1583 (2007).
[7] R. G. Clarkson, P. von Brentano, and H. L. Harney, Nucl. Phys. A **161**, 49 (1971).
[8] A. Heusler, H. L. Harney, and J. P. Wurm, Nucl. Phys. A **135**, 591 (1969).
[9] M. Löffler, H. J. Scheerer, and H. Vonach, Nucl. Instrum. Methods B **111**, 1 (1973).
[10] J. Ott, H. Angerer, T. von Egidy, R. Georgii, and W. Schauer, Nucl. Instrum. Methods A **367**, 280 (1995).
[11] H.-F. Wirth, Ph.D. thesis, Techn. Universität München (2001) [http://tumb1.biblio.tu-muenchen.de/publ/diss/ph/2001/wirth.html].
[12] B. D. Valnion, V. Yu. Ponomarev, Y. Eisermann, A. Gollwitzer, R. Hertenberger, A. Metz, P. Schiemenz, and G. Graw, Phys. Rev. C **63**, 024318 (2001).
[13] A. Heusler *et al.*, in Changing Facets of Nuclear Structure, *Proceedings of the 9th International Spring Seminar on Nuclear Physics*, edited by A. Covello (World Scientific, Singapore, 2008), p. 293, [http://www.worldscibooks.com/physics/6667.html].
[14] A. Heusler *et al.*, in *Proceedings of the 23th International Nuclear Physics Conference (INPC2007)*, Tokyo (2007), Vol. 2, p. 254; [http://inpc2007.riken.jp/F/F4-heusler.pdf].
[15] National Nuclear Data Center, Brookhaven, Evaluated Nuclear Structure Data File [http://ie.lbl.gov/ensdf/].
[16] A. Heusler and P. von Brentano, Ann. Phys. (NY) **75**, 381 (1973).
[17] A. Heusler [http://www.mpi-hd.mpg.de/personalhomes/hsl/208Pb_eval/appendix_A.pdf].
[18] G. Audi, A. H. Wapstra, and C. Thibault, Nucl. Phys. A **729**, 337 (2003).
[19] A. Bohr and B. R. Mottelson, *Nuclear Structure* (W. A. Benjamin, New York, 1969), Vol. I.
[20] A. Bohr and B. R. Mottelson, *Nuclear Structure* (W. A. Benjamin, New York, 1969), Vol. II.

[21] K. Heyde, M. Waroquier, H. Vincx, and P. J. Brussaard, Nucl. Phys. A **234**, 216 (1974).
[22] M. Yeh, P. E. Garrett, C. A. McGrath, S. W. Yates, and T. Belgya, Phys. Rev. Lett. **76**, 1208 (1996).
[23] K. Vetter *et al.*, Phys. Rev. C **58**, R2631 (1998).
[24] B. A. Brown, Phys. Rev. Lett. **85**, 5300 (2000).
[25] W. T. Wagner, G. M. Crawley, G. R. Hammerstein, and H. McManus, Phys. Rev. C **12**, 757 (1975).
[26] C. K. Bockelman, D. G. Kovar, Nelson Stein, Nucl. Phys. A **231**, 266 (1974).
[27] W. Dünnweber, E. R. Cosman, E. Grosse, and W. R. Hering, Nucl. Phys. A **247**, 251 (1975).
[28] O. Hansen, N. Stein, D. G. Burke, E. R. Flynn, J. D. Sherman, J. W. Sunier, and R. K. Sheline, Nucl. Phys. A **277**, 451 (1977).
[29] A. Heusler, G. Graw, R. Hertenberger, H.-F. Wirth, R. Krücken, C. Scholl, and P. von Brentano, Eur. Phys. J. A **44**, 233 (2010).
[30] P. Grabmayr, G. Mairle, U. Schmidt-Rohr, G. P. A. Berg, J. Meissburger, P. von Rossen, and J. L. Tain, Nucl. Phys. A **469**, 285 (1987).
[31] M. Schramm *et al.*, Phys. Rev. C **56**, 1320 (1997).
[32] P. Grabmayr, private communication (2008). Four spectra of ^{209}Bi(d,^{3}He) and four spectra of ^{208}Pb(d,^{3}He) taken with the Big Karl magnetic spectrograph at Jülich in 1981 under similar conditions as [30] are reanalyzed by GASPAN [33] and recalibrated by NDS2007 [6].
[33] F. Riess/GASPAN [http://homepages.physik.uni-muenchen.de/~Riess/gaspan/].
[34] A. Heusler, G. Graw, R. Hertenberger, H.-F. Wirth, P. von Brentano, Maier-Leibnitz Laboratorium, Annual Report, Universität München (2004) [http://www.bl.physik.uni-muenchen.de/bl_rep/jb2004/p021.ps].
[35] J. P. Connelly, D. J. DeAngelis, J. H. Heisenberg, F. W. Hersman, W. Kim, M. Leuschner, T. E. Milliman, J. Wise, and C. N. Papanicolas, Phys. Rev. C **45**, 2711 (1992).
[36] M. Rejmund, M. Schramm, and K. H. Maier, Phys. Rev. C **59**, 2520 (1999).
[37] A. Heusler, G. Graw, R. Hertenberger, H.-F. Wirth, P. von Brentano, Maier-Leibnitz Laboratorium, Annual Report, Universität München (2003) [http://www.bl.physik.uni-muenchen.de/bl_rep/jb2003/p21.ps].